# Less is more - loss of EGFL7 improves memory by upregulation of VEGF-D

Verica Vasić[1,2,*], Kathrin Barth[3,*], Frank Bicker[1,2], Ulrike Schumann[3], Christine Maurer[1,2,4], Nora Heinig[3], Cora Röhlecke[3], Ute Nimtschke[3], Lana Schumann[4], Matthias Meinhardt[5], Thomas Mittmann[2,6], Konstantin Radyushkin[2,7], Jan Baumgart[8], Stefan Tenzer[9,10], Frauke Zipp[2,10,11], Irmgard Tegeder[4,§], Mirko HH Schmidt[3,§]

[1] Institute of Microscopic Anatomy and Neurobiology, University Medical Center of the Johannes Gutenberg University Mainz, Mainz, Germany;

[2] Focus Program Translational Neuroscience (FTN), University Medical Center of the Johannes Gutenberg University Mainz, Mainz, Germany;

[3] Institute of Anatomy, Medical Faculty Carl Gustav Carus, Technische Universität Dresden School of Medicine, Dresden, Germany;

[4] Institute of Clinical Pharmacology, Goethe-University Hospital Frankfurt am Main, Germany;

[5] Institute of Pathology, University Hospital Carl Gustav Carus, Technische Universität Dresden, Dresden, Germany;

[6] Institute of Physiology, University Medical Center of the Johannes Gutenberg University Mainz, Mainz, Germany;

[7] Mouse Behavior Outcome Unit, Johannes Gutenberg University Mainz, Mainz, Germany;

[8] Translational Animal Research Center (TARC), University Medical Center of the Johannes Gutenberg University Mainz, Mainz, Germany;

[9] Institute of Immunology, [10] Focus Program Immunotherapy (FZI), University Medical Center of the Johannes Gutenberg University Mainz, Mainz, Germany;

[10] Focus Program Immunotherapy (FZI), University Medical Center of the Johannes Gutenberg University Mainz, Mainz, Germany;

[11] Department of Neurology, Rhine-Main Neuroscience Network (rmn$^2$), University Medical Center of the Johannes Gutenberg University Mainz, Mainz, Germany.

* Verica Vasić and Kathrin Barth contributed equally to this work.

§ Irmgard Tegeder und Mirko HH Schmidt jointly supervised this work.

Running head: EGFL7 governs learning and memory

**Correspondence to**

Prof. Mirko HH Schmidt, MD, PhD

Institute of Anatomy

Medical Faculty Carl Gustav Carus

Technische Universität Dresden

Fetscherstr. 74

D-01307 Dresden, Germany

Phone: 0049 351-458-6110

Fax: 0049 351-458-6303

Email: mhhs@mailbox.tu-dresden.de

## Abstract

Neural stem cells reside in a specialized neurogenic niche of the hippocampus termed the subgranular zone. Throughout life, they give rise to adult-born neurons in the dentate gyrus thereby contributing to learning and memory. Here, we report that neurons together with neural stem and precursor cells secrete the neurovascular protein epidermal growth factor-like protein 7 (EGFL7) to shape this niche. EGFL7 knock-out *in vivo* promoted adult neurogenesis generating neurons forming additional spines which permanently integrated into the neural circuit until old age. RNA-sequencing identified the cytokine VEGF-D as a major molecular driver of this process *in vivo*. In behavioral studies EGFL7 knock-out mice displayed stronger maintenance of memory suggesting longer-lasting spatial memory and improved memory consolidation in the hippocampus by modulation of pattern separation in young and aged mice. Taken together, EGFL7 is an upstream regulator of the VEGF-D in adult neurogenesis and a key regulator of learning and memory.

## Introduction

In the 1960s, *de novo* formation of neurons in the adult brain was described in rats and cats(1). Since then, this biological paradigm has been confirmed in the brain of various species, e.g., songbirds(2), rodents(1, 3, 4) and humans(5-9), and has been termed adult neurogenesis. In rodents it occurs in the subgranular zone (SGZ) of the dentate gyrus (DG) of the hippocampus (HC) and in the subventricular zone (SVZ) of the lateral walls of the lateral ventricles(10). In particular, the HC is associated with neurological deficits and psychiatric diseases due to its implication in learning and memory(11). In spite of the fact that the number of adult-born neurons is low compared to the total number of neurons in the DG, the continuous production of new neurons by adult neurogenesis during a lifetime contributes to the maintenance of cognitive function and brain plasticity(8, 12-14).

The electrophysiological characteristics of young adult-born neurons differ from those of mature cells in the DG. They are hyperexcitable and highly plastic and are therefore preferentially recruited into novel memory traces(15). These cells originate from neural stem cells (NSCs) residing in the adult SGZ which are mostly quiescent but show a typical radial morphology. NSCs are also referred to as radial glia-like (RGL) or type 1 cells giving rise to intermediate progenitors with a glial (type 2a) and a neuronal (type 2b) phenotype. Subsequently, type 3 cells (neuroblasts) are formed which exit the cell cycle and mature into granule cells (GCs)(16, 17). GCs extend their dendrites into the molecular layer and project their axons to the CA3 region of the hippocampus, thereby orchestrating tri-synaptic signalling circuits(18) and modulating learning and memory(19).

Adult neurogenesis in the HC is regulated by biochemical or physiological factors(15), by environmental cues and by experience(20). In particular, the Notch signalling pathway is a key regulator of NSC maturation and neuron formation(21) in adult neurogenesis(22). Notch regulates proliferation as well as cell fate decisions of NSCs and intermediate progenitors cells(23). A conditional knock-out (KO) of Notch in NSCs as well as the depletion of RBPj, the transcription factor activated by Notch, caused a reduction in the amount of adult-born neurons, NSCs and intermediate

progenitors(23, 24). Notch receptors become activated by canonical Notch ligands of the Delta- and Jagged-type(25).

Previously, we have shown that this interface is modulated by the non-canonical Notch ligand epidermal growth factor-like protein 7 (EGFL7), which antagonized Jagged1-induced Notch signalling(26) but stimulated Dll4-induced(27) activation of Notch receptors in NSCs. In this way, EGFL7 governed adult neurogenesis and network activity in the olfactory bulb (OB) which caused hyposmia upon KO in mice. EGFL7 expression increased in cells of the maturing brain until young adulthood and remained at high levels until old age(28). In the SVZ, EGFL7 is produced at high levels by NSCs but it is also secreted by neurons and endothelial cells(29) throughout the adult brain(30),(31). These findings prompted us to investigate whether or not EGFL7 governs adult neurogenesis in the SGZ of the HC. In this study, we show where EGFL7 is expressed in the HC of mice and man, how it governs adult neurogenesis in the SGZ and which consequences a loss-of-EGFL7 has for learning and memory.

## Materials and methods

### Animals

Animal experiments were approved by the Landesuntersuchungsamt Koblenz, Rhineland-Palatinate, Germany, the Regierungspräsidium Darmstadt, Hesse, Germany and the Landesdirektion Chemnitz, Saxony, Germany (permit number TVA G16-1-002 and TVV 56/2020). Experiments were conducted according to the German Animal Welfare Law and the Directive 2010/63/EU for the protection of animals used for scientific purposes and followed the ARRIVE and GV-SOLAS guidelines for research in behaving animals. Mice were housed in climate-controlled, pathogen-free conditions at the Transgenic Animal Research Center (TARC, University Medical Center Mainz, Germany), the central animal research facility (ZFE, University Hospital, Frankfurt, Germany) and the Experimental Center of the Medical Theoretical Center (MTZ, Medical Faculty Carl Gustav Carus, Dresden, Germany) on a 12 h light-dark cycle with free access to food and water.

### Mouse lines

**C57BL/6J** inbreed mice (control WT mice) were purchased from Janvier Labs (Le Genest-Saint-Isle, France).

**Constitutive *EGFL7-/-* mice** were generated and kindly provided by Weilan Ye, (Genentech, San Francisco, USA) and applied as previously described(32). KO was achieved by insertion of a retroviral gene trap vector upstream of intron 2 of the *Egfl7* gene. The insertion led to silencing of EGFL7 translation as transcripts initiated from the inserted vector contain stop codons in all three frames.

***EGFL7-/-;Thy1-GFP.*** *Thy1-GFP* mice carry an enhanced green fluorescent protein (GFP) transgene under the control of a modified *Thy1* promoter were crossed with *EGFL7-/-* mice, enabling fluorescent labeling of neural tissues, upon loss or presence of EGFL7.*Thy1-GFP* mice were also used for flow cytometry sorting of neurons from the HC.

***EGFL7 fl/fl;Ascl1-CreERT2.*** In order to allow for a cell type-specific and tamoxifen-inducible KO of EGFL7, conditional *EGFL7 fl/fl* mice were generated by insertion of loxP cassettes upstream of exon 3 and downstream of exon 7 (ingenious targeting laboratory, Ronkonkoma, USA). This way Cre-mediated recombination removed all putative start codons from the *Egfl7* gene. Mice were crossed with *Ascl1-CreERT2*(33) animals in which the entire coding region of *archaete-scute complex homolog 1* (*Ascl1*) is replaced by a CreERT2 fusion protein allowing for the tamoxifen-induced deletion of EGFL7 in neural progenitors.

***EGFL7 fl/fl;DCX-CreERT2.*** *DCX-CreERT2* mice were created by Prof. Wolfgang Wurst(34) allowing doublecortin (*DCX*) promoter-driven deletion of *Egfl7* in *DCX*-positive immature neuronal cells in the CNS. A fragment containing the Cre-ERT2 sequence was inserted into a plasmid containing the human *DCX* promoter, and the targeting vector of 7.7 kb was inserted upstream of the 3' UTR of *DCX*.

***EGFL7 fl/fl;EIIa-Cre.*** *EGFL7 fl/fl* animals were crossed with EIIa-Cre(35) pan-deleter animals expressing Cre under the adenovirus promotor EIIa, allowing for the deletion of EGFL7 in, among others, germ line cells. This alternative constitutive EGFL7 KO model was applied in a set of behavioral studies to exclude strain-specific artifacts.

## Mouse treatments

**BrdU, CldU**. A 10 mg/ml solution of bromdesoxyuridin (BrdU) or 5-chloro-2□-deoxyuridine (CldU) was prepared and 100 µl of injection solution were injected intraperitoneal (ip). **IdU**. 500 µl of a 2 mg/ml 5-iodo-2'-deoxyuridine (IdU) solution were injected ip. Hence, mice received about 1 mg base analog per animal (approximately 40 mg/kg). **Tamoxifen**. Mice received daily injections of tamoxifen in peanut oil/ethanol (9:1) as a vehicle ip at a dose of 3 mg/20g body weight for three consecutive days.

## Osmotic pump implantation and intraventricular infusion

8-week-old male C57BL/6J mice (n = 6) were anaesthetized by the administration of a ketamine-xylazine mixture ip (100 µl per 10 g body weight, ketamine 200 mg/kg, xylazine 20 mg/kg, both in a

0.9% sodium chloride solution). At the surgical tolerance stage, an incision was made with a scalpel above the position of the bregma, and the skull was exposed. A 1-mm diameter hole was drilled at the following coordinates: 0 mm anteroposterior, 0.8 mm lateral to bregma. Subsequently, a catheter was placed through the hole 2 mm below the surface of the skull into the lateral ventricle and connected to a mini-osmotic pump (2001, Alzet, Cupertino, CA, USA) which was placed into a subcutaneous skin dorsal fold. The pump delivered 1 µg/d of recombinant purified VEGF-D (R&D systems, Minneapolis, MN, USA) into the ventricle for 7 d at 1 µl/h. The wound was closed and mice were allowed to recover. Mice received IdU solution (200 mg/kg body weight) ip at d1 or CldU solution (200 mg/kg body weight) at d6 after surgery. Mice were sacrificed and tissue prepared at d7.

## Tissue preparation

Mice were anaesthetized by the administration of a ketamine-xylazine mixture ip (100 µl per 10 g body weight, ketamine 450 mg/kg, xylazine 48 mg/kg, both in a 0.9% sodium chloride solution). Subsequently, mice were perfused transcardially with phosphate-buffered saline (PBS), followed by 4% paraformaldehyde in 1x PBS. The high dose of ketamine-xylazine represents an overdose to kill the animals by perfusion.

Brains were removed, fixed in 4% paraformaldehyde in PBS at 4 °C for 24 h, subsequently transferred into 15% sucrose and finally, into 30% sucrose solution in PBS for cryoprotection. Brains were cut on a vibratome (HM650V, Thermo Fisher Scientific, Waltham, USA) to obtain 40-µm thick sections which were stored in cryoprotective solution at −20 °C. Alternatively, brains were embedded in Tissue-Tek O.C.T. solution (Sakura Fintek, Torrance, CA, USA), frozen on dry-ice and stored at −80 °C until further processing. Coronal cryosections were prepared at a thickness of 10 µm and stored at −20 °C.

## Primary neuronal culture

Primary neuronal cultures were prepared from the hippocampus of 1 day old EGFL7$^{-/-}$ and WT pups (p1). Briefly, the hippocampus was dissected and freed of meninges. The cells were dissociated by trypsinization (0.25% for 20 min at 37°C) with additional DNAse, followed by trituration with a fire-polished Pasteur pipette and plated onto poly-L-lysine-coated 24 well plates containing minimal essential medium (MEM) with 10% horse serum and 3% penicillin/streptomycin. Three hours after seeding, the medium was changed to Neurobasal medium. Cultures were maintained at 37 °C and culture media were exchanged every 3 days. The cells were washed and fixed after one week and stained with Map2 antibodies to label dendrites. The numbers and lengths of dendrites were analyzed in ImageJ using the Simple Neurite Tracer plugin.

## Neural stem cell assays

Primary neurosphere cultures were prepared from adult mice (8-12 weeks old) as previously described(27). Mice were sacrificed by cerebral dislocation. Brains were removed and the forebrain was opened under sterile conditions to remove the hippocampus. Tissue was enzymatically dissociated by incubation in Leibowitz L-15 medium containing 0.8 mg/ml papain and 0.5 mM Ethylenediaminetetraacetic acid (EDTA; dissociation medium, pre-activated at 37 °C for 30 min) at 37 °C for 30 min. After centrifugation for 3 min at 300 *g*, the supernatant was removed and the tissue was resuspended in ovomucoid inhibitor (Worthington, Lakewood, CO, USA). Cells were triturated with a fire-polished Pasteur pipette, collected by centrifugation for 3 min at 300 g, resuspended in NSC medium (DMEM/F-12 medium containing 1 mM HEPES, 10 µg/ml penicillin, 10 µg/ml streptomycin, 1 x B27 supplement, 20 ng/ml EGF and 20 ng/ml FGF) and were plated in T75 flasks. Cells were incubated at 37 °C and 5% $CO_2$ and were passaged every 5 d by enzymatic dissociation with accutase (PAA, Egelsbach, Germany) at 37 °C for 10 min under vigorous shaking. For analysis of sphere size, neurospheres were grown for 5 d *in vitro* at clonal density. The number of formed spheres and their diameters were determined using an IX70 microscope (Olympus, Hamburg,

Germany). Statistically significant differences between genotypes were calculated using two-sided, unpaired Student's t-tests.

## Cell cycle analysis and apoptosis assay

Cell cycle analysis of ploidy by flow cytometry was performed using Hoechst 33342 dye (Sigma Aldrich, St. Louis, MO, USA). HC-derived NSCs were incubated in 10 µg/ml Hoechst 33342 solution for 10 min at 37 °C in culture medium. Incorporated Hoechst 33342 was excited using an UV Laser. Cell scatters were gated according to fluorescence intensity and plotted as histograms. The area parameter histogram was used to determine the percentage of cells in G1, S or G2/M phase. Mann-Whitney *U*-test was used for statistical analysis. Caspase 3 staining was used for the assessment of apoptosis. Images were obtained with a TCS-SP5 confocal microscope (Leica, Wetzlar, Germany).

## Antibodies and stainings for flow cytometry

Cell populations were identified by flow cytometry as previously described(36). Animals were sacrificed by cervical dislocation; brains were immediately removed and the HC was micro-dissected. Pooled tissue samples (5 mice per sample) were digested with papain plus DNase and mechanically dissociated as previously described(36). Cells were stained for 30 min at 4 °C in the dark in PBS using the following antibodies and conjugates: qNSCs and aNSCs were discriminated by a combination of PE-conjugated anti-mGLAST (1:50, clone ACSA-1, Miltenyi Biotec, Bergisch Gladbach, Germany), APC-conjugated anti-mCD133 (1:75, clone 13A4, Invitrogen, Darmstadt, Germany), EGF, biotinylated, complexed to Alexa Fluor 488 streptavidin (Alexa Fluor™ 488 EGF complex) (1:100, Invitrogen), APC-Cy7 rat anti-mCD45 (1:200, Becton Dickinson, Franklin Lakes, NJ, USA) and APC-Cy7 anti-mTer119 (1:100, Biolegend, San Diego, CA, USA). In order to sort neural stem and precursor cells, neuroblasts, neurons or endothelial cells from the HC by flow cytometry a fluorescence-activated cell sorting device type Aria II (BD Biosciences) was used, Alexa Fluor 488-conjugated GFAP (rabbit anti-mGFAP

1:100, clone G-A-5, Sigma), PE-Cy7-conjugated rat anti-mCD133 (1:100, clone 315-2C11, Biolegend), Biotin-xx-Conjugated EGF (1:200, Thermo Fisher Scientific) plus Streptavidin-PE (1:100, BD Biosciences, San Jose, CA, USA), eFluor405-conjugated rat anti-mCD24 (1:100, BD Biosciences), PE-conjugated rat anti-mCD31 (1:50, clone MEC133, BD Biosciences) or Thy1-GFP mice were applied and cells were collected in PBS.

## RNA isolation and reverse transcription

Mouse brains were mechanically disrupted using a mortar and pestle precooled in liquid nitrogen. Disruption of neurosphere cultures was achieved using Trizol Reagent (Invitrogen) according to the manufacturer's instructions. Disrupted tissues and cells were further homogenized by QIAshredder columns (Qiagen, Hilden, Germany). Cells sorted by flow cytometry were lysed in RLT buffer (Qiagen). RNA was purified using RNeasy mini kit (Qiagen) according to the manufacturer's instructions. The concentration and purity of RNA were determined using the Bioanalyzer 2000 automated electrophoresis system (Agilent, Santa Clara, CA, USA). cDNA was synthesized using oligo-d(T) primers and avian reverse transcriptase (iScript cDNA Synthesis Kit, Bio-Rad, Hercules, CA, USA) according to the manufacturer's instructions.

## Quantitative reverse transcriptase-polymerase chain reaction (qRT-PCR)

qRT-PCR was performed using SYBR Green fluorescein mix (Thermo Fisher Scientific), using 2 ng of template cDNA and 1 pmol of gene-specific primers per reaction. PCR reaction and amplicon detection were performed by the iCycler real-time PCR system (CFX Connect RT-PCR System, Bio-Rad). Quantification of expression was normalized according to the relative levels of cDNA of the housekeeping genes RNA polymerase II (RNAPII) and ribosomal protein S13 (Rps13). Primer sequences are listed in Supplementary Table 1. Statistical analysis was performed using Student´s t-test.

### Fluorescence *in situ* hybridization (FISH)

Brain sections were cut on a cryostat at 10 µm thickness (Cryostat CM 1900; Leica), dried for 30 min at 37 °C and stored at -20 °C until further processing. FISH was performed using QuantiGene ViewRNA ISH Cell Assay (Affymetrix, Santa Clara, CA, USA). For multiplexing, Type-1 and Type-6 probes were combined. Images were captured using a confocal microscope (SP8, Leica).

### Immunofluorescence (IF) and immunoperoxidase staining

Sections were mounted on glass slides or were used free-floating for staining. Subsequent to a PBS wash, antigens were retrieved in preheated citric acid for 30 min. After washing, sections were treated with hydrochloric acid and borate buffer. Blocking was performed at RT for 1 h in 10% goat or donkey serum plus 0.01% Triton X-100. Primary antibodies (rat anti-BrdU, 1:100, Abcam; mouse anti-BrdU, 1:100,BD Biosciences; mouse anti-Nestin, 1:300, Millipore; rabbit anti-GFAP, 1:400, Dako; rabbit anti-Ki67, 1:100, Abcam; rabbit anti-Stathmin1, 1:250, Thermo Fisher; rabbit anti-Mash1, 1:100, Abcam; goat anti-DCX, 1:250, Santa Cruz; rabbit anti-DCX, 1:100, Abcam; rabbit anti-NeuN, 1:100, Abcam; rabbit anti-VEGF-D, 1:250, Thermo Fisher) were applied at a concentration of 10 µg/ml at RT for 10 min after washing. Sections were again washed with 10 x PBS and mounted in Fluoromount-G (Invitrogen). Images were captured using a confocal microscope (SP5 or SP8, Leica). Statistical analysis was performed using the Mann-Whitney *U*-test.

Immunoperoxidase staining of paraffin sections from human HC probes (n = 3) was performed using the ABC technique. Briefly, 4-µm thick sections were deparaffinized, dried overnight and microwaved in 0.01 M sodium citrate buffer after washing in phosphate buffered saline (PBS, pH 7.4). A conventional immunohistochemical procedure was followed using a commercially available detection system (Vectorstain Elite Kit, Vector Laboratories, Burlingame, USA). Peroxidase activity was visualized using 3'-3'diaminobenzidine, tissue was counterstained by hemalum. As primary antibody a polyclonal rabbit anti-human EGFL7 antibody (1:50, ReliaTech GmbH) was applied. Primary antibodies were replaced by PBS or by nonspecific rabbit IgG as negative controls. Human

placenta tissue from normal pregnancies (tissue collection of the Department of Anatomy, Dresden, Germany) was used as a positive control.

## Dendritic spine analysis

Eight weeks old and 20 weeks old *EGFL7*-/-;*Thy1-GFP* mice (n = 3) were perfused and fixed in 4% PFA. Forty µm vibratome slices were stained with a free floating technique (without steaming) using anti GFP-Alexa 488 (1:500). A minimum of 15 images were captured per mouse DG using a Leica TCS-SP5 confocal microscope at 63x magnification and zoom 6. The images were processed and analyzed in ImageJ, and the numbers of spines and their morphology were analyzed in Neuron Studio. Statistical analysis was performed using the Mann Whiney *U* test.

## Statistical analysis of anatomical and biological data

Data are presented as mean ± standard deviation (SD) unless explained otherwise. Statistical analyses were performed using GraphPad Prism 8.0 software (Statcon, Witzenhausen, Germany). Student's t test or Mann-Whitney *U*-test was used for statistical analysis of three or more biological replicates per experiment; $p < 0.05$ was considered significant. All experiments and analyses were carried out without knowledge of the genotype or treatment group. Parametric data were analyzed using an unpaired two-tailed Student's t-test. Non-parametric data or low sample sizes were analyzed with the Mann-Whitney *U*-test. Analysis of behavioral data is explained below. Statistical methods are described in figure legends or specific experimental procedures.

## RNA-sequencing

Transcriptomic analyses consisted of two sequential experiments. The first set comprised NSCs of SVZ and HC of *EGFL7*-/- and WT litters (n = 4), the second comprised neurospheres of NSCs of HC (n=4), only. Alignments and analyses were done for each data set and subsequently combined. RNA from NSCs was isolated after 3 d (SVZ) or 5 d (HC). RNA concentration and quality were determined

using Bioanalyzer 2000 and Nanodrop. RNA-sequencing (RNA-Seq) was performed by CeGaT (Tübingen, Germany) according to standard protocols. Briefly, TruSeq RNA Sample Prep Kit (Illumina, San Diego, CA, USA) was used with 0.5 µg of total RNA for the construction of sequencing libraries. Libraries were prepared according to Illumina's instructions and SureSelectXT Mouse All Exon enrichment kits (Agilent) were used. Sequencing of 2x 100 bp was done on NovaSeq6000 (Illumina) with a sequencing depth of 50 Mio reads per sample.

Starting with demultiplexed fastq.gz files, the fastqc program FASTQC (Version 0.11.5-cegat)(37) was applied to assess sample quality, and subsequently the alignment was performed with SeqMan NGen 15 (Lasergene, Madison, WI, USA) using the reference genome mm10 provided from UCSC (GRCm38)(38) as template, a minimum read length of 35 bp and automatic adapter trimming. Results were displayed with ArrayStar 15 (Lasergene) including the amount of mapped reads, target length, source length and position, strand, genes and gene IDs, annotated according to the mm10 assembly, and reads were normalized according to RPKM. Alternative DEseq2 normalization yielded equivalent results. Normalized reads were analyzed with ArrayStar, which uses general linear models to assess differential expression. Genes were filtered for at least 10 valid values out of a total of 20 samples with normalized reads > 0.05 (combined dataset) to exclude low expression genes. Data were log2 transformed, single missing values were set to an auto-calculated minimum, and results were displayed as scatter plots, MA-plots and Volcano plots, the latter showing the log2 difference, i.e., fold change (positive for upregulated genes and negative for downregulated genes) versus the -log10 of the t-test P value. The P value was set at 0.05 and adjusted according to Benjamini-Hochberg. Hierarchical clustering was employed to assess gene expression patterns using Euclidean distance metrics. Results were displayed as heat maps with dendrograms.

The differential expression analyses were first done for each experiment separately, and the agreement was assessed with Venn diagrams of top regulated genes (criteria $P < 0.05$, 1.5-fold change). The datasets were then combined, re-normalized and reanalyzed to gain statistical power. Functional analyses are based on the combined analysis. Gene set enrichment analyses (GSEA)

(http://www.gsea-msigdb.org)(39) were used to assess functional implications of up- or downregulated gene networks and for gene ranking based on fold difference, P value and abundance. Leading edge 50 up- and downregulated genes according to GSEA are displayed as heatmaps.

## Behavioral analyses

### Morris water maze (MWM)

Spatial learning and memory were assessed in a Morris water maze(40) in a cohort of 19 *EGFL7*-/- and 33 WT control mice. The bath tank (diameter 1.2 m, depth 0.4 m) was filled with opaque water (25± 1°C, depth 0.3 m) and the escape platform (10x10 cm) was submerged 1 cm below the surface. The swim patterns were monitored by the PC-based video-tracking system from Ethovision (Noldus Inc., Netherland). The escape latency, swim speed, path length, and swimming paths were recorded. Mice were trained to swim to a clearly "visible platform" that was marked with a 15 cm high black flag during the first 2 d. The position of the visible platform was changed pseudo-randomly (non-spatial learning). Extra-maze cues were hidden during these trials. After 2 d of "visible platform" training, the "hidden platform" training (spatial training) was performed for 8 d. The mice had to find a hidden platform (the flag was removed) that was located at the centre of one of the four quadrants of the pool. The location of the platform was fixed throughout the running test. Mice had to navigate using extra-maze cues that were placed on the walls. Every day they received four trials with an inter-trial interval of 5 min. The mice were placed into the pool facing the sidewall randomly at one of four start locations and allowed to swim until they found the platform, or for a maximum of 90 s. Mice that failed to find the platform within 90 s were guided to the platform. The animal then remained on the platform for 20 s before being removed from the pool. After completion of the "hidden platform" training, a trial without platform was done to assess the spatial memory. For this, mice were allowed to swim freely for 90 s. The percentage of time spent in each quadrant of the pool and the number of times crossing the former position of the platform were recorded.

## Barnes maze spatial learning

A cohort of 15 *EGFL7 fl/fl;EIIa-Cre* and 15 *EGFL7 fl/fl* female mice were used for analysis of spatial learning in a Barnes maze (TSE, Bad Homburg, Germany). The animals had no prior experience of learning tasks and were 27-35 weeks old at the onset of adaptation. A classical avoidance-based test and a reward-based two-choice paradigm were employed sequentially with an interval of 35 weeks in between, the latter with a subgroup of nine and eight animals per group. The maze was divided into center, target (i.e., escape/rewarding box), opposite and neutral zones. The protocols consisted in three phases: habituation, target acquisition, and reversal or extinction learning. During habituation, mice were placed in the middle of the maze under a transparent cylinder for 20 s, and were then guided to the target hole, where they were allowed to enter the shelter. If they did not escape within 3 min, they were gently nudged into the box and allowed to stay there for 1 min. For the two-choice Barnes maze, mice were put on a mild restriction diet to increase appetite for the reward, which was placed in one of two boxes in the same quarter, two holes apart, while the other was empty. The habituation was performed on 3-4 consecutive days with two trials per day. In the target acquisition phase (3-4 d, 1 trial per day) mice were placed in the middle of the maze under an opaque cylinder for 20 s and then allowed to freely explore the maze for 5 min to find and enter the escape/reward box. In the subsequent classical REVERSAL learning (4 d, 1 trial per day), the escape box was moved to the opposite side of the maze. In the two-choice reward extinction period, only the reward was removed but positions of the boxes were maintained. EthoVision XT 11.5 (Noldus, Wageningen, Netherlands) was used for video tracking and analysis. Trial duration, distance moved, velocity, zone visits and cumulative duration in each zone were recorded.

## IntelliCage

The IntelliCage experiments were performed with 16 female mice per genotype (*EGFL7*-/- or WT), which were 11-16 weeks old at the onset of the experiments; eight mice were housed per cage. The IntelliCage (NewBehavior AG, Zürich, Switzerland(41-44) consists of four operant corners, each with

two water bottles, sensors, light-emitting-diodes (LEDs) and doors that control access to water bottles. Mice were tagged with radio-frequency identification (RFID)-transponders to record corner visits, nosepokes and lickings to observe the behavior in pre-designed tasks, summarized in Supplementary Table 2 and 3. Mice were adapted to the system for 3 d with free access to every corner, with all doors open, and water and food ad libitum (free adaptation, FA). FA was followed by a 6 d nosepoke adaptation period (NP), during which the doors remained closed, the first nosepoke of the visit opened the door for 5 s and in order to drink more, the animals had to leave the corner and start a new visit.

### Place avoidance acquisition (PAA) and extinction (PAEx)

In PAA, mice had to learn to avoid one punished corner, which was randomly assigned to each 4 mice per cage. The punishment consisted in an air puff (~ 0.8 bar, 1 s), and it was coupled with red LED upon NP on the forbidden door, which remained closed. The avoidance acquisition lasted for 24 h. At completion, mice returned to their home cages for 1 d with water restriction overnight prior to their return to their IntelliCage for the analysis of the extinction of the avoidance behavior (PAEx). The IntelliCage was not cleaned to maintain environmental and olfactory cues. In PAEx, all doors opened upon nosepoke and no air-puff was applied. Only the red LED still reminded of the previously "punished" corner and was switched on upon visit of a previously forbidden corner.

### Place preference learning

After a home cage interval, the mice returned to the IntelliCage, were re-adapted and were then adapted to daily drinking sessions (DS) for 15 d, which allowed access to the bottles only for 2 x 2 h per day from 11 a.m. – 1 p.m. and 4 – 6 p.m. (referred to as "module active times"). The restriction increases the motivation to learn and allows for assessment of preference maintenance outside of the "module active times". The day-patterns were maintained during subsequent learning tasks. In the first "place preference learning" task, mice had to learn to prefer a specific corner, where they

got access to the water reward on both sides (PPL). Correct corner visits were coupled with green LED. Each four mice per cage were assigned to one corner. The PPL module was active only during the respective drinking sessions and lasted for 7 d. Subsequently, the challenge was increased by allowing bottle access only on one side in the rewarding corner (PPL1c1s). After 7 d, both corner and side were switched to the opposite side (PPL1c1s-REVERSAL). After relearning the corner for 7 d, a PPL-switch protocol followed, in which the correct corner switched back and forth between opposing corners during the morning and afternoon drinking sessions.

## Statistical assessment of behavioral experiments

Behavioral data are presented as mean ± SD or mean ± SEM, the latter for behavioral time courses, as specified in the respective figure legends. Data were analyzed with Graphpad Prism 6 or 8 and FlowR for IntelliCage experiments. Data were normally distributed, unless stated otherwise. Time course data or multifactorial data were submitted to two-way analysis of variance (ANOVA) using the factors 'time' and 'genotype'. In case of significant differences, groups were mutually compared at individual time points using post hoc t-tests and adjustment of the P value according to Šidák or without adjustment for between subject factor analyses of two groups. Asterisks in figures show significant differences between genotypes. For testing the null-hypothesis that groups were identical, areas under the curve (AUCs) were calculated using the linear trapezoidal rule and AUCs were compared per unpaired two-tailed t-tests.

In the IntelliCage, numbers of visits, nosepokes and licks show overall activity and drinking behavior. To assess time courses of success, the percentages of correct visits or nosepokes during the active module-times (as defined by the drinking sessions, 11:00 AM – 01:00 PM and 04:00 – 06:00 PM each day) were plotted versus time. The default modules, in which doors remained closed - outside the drinking sessions - were analyzed to assess the maintenance of rewarding corner preference. To assess the number of trials needed to achieve learning success, a probability test was used with the success criterion set to 0.35 for experiments with a random success of 0.25. Type 1 and type 2 errors

were set to 0.05. The cumulative probability to achieve the respective criterion of success was plotted versus trial number to assess the proportion of memorizers in each group.

## IntelliCage (IC) in old mice

IntelliCage behavior and cognitive performance were analyzed with old *EGFL7 fl/fl;EIIa-Cre* and *EGFL7 fl/fl* female (n=14-15 per genotype) which were 71-78 weeks old at the onset of the experiments. Mice were assigned pseudo-randomly to IC1 and IC2 to achieve balanced numbers per cage per genotype. The IntelliCage protocol consisted in 4 days free adaptation (FA), three weeks nosepoke adaptation (NP), 7d place preference learning & 7d reversal learning without stress (PPL1 & Reversal1), 7d place preference learning & 7d reversal learning in combination with mild stressors (CUMS) to disrupt circadian rhythms (PPL2 & Reversal2), and finally again five weeks of an unrestricted NP protocol without stress to observe the post-stress period. CUMS stressors consisted in providing bits of food every hour after overnight fast, darkness for 36 h, repeated change of bedding, and removal of red houses during daytime. The stressors were applied in unpredictable order for 14 days during PPL2 & REVERSAL.

## Touchscreen Chambers

Bussey–Saksida touchscreen equipment (Campden Instruments Ltd/Lafayette Instruments) was used as described(45).The trapezoidal operant chamber consists of an infrared touchscreen spanning the wider end of the trapezoid, a perforated floor and a peristaltic liquid reward supply at the narrow end of the trapezoid. Presentation of stimuli, nosepokes on the screen and capture of the behavior with video cameras were controlled by Lafayette ABET II software. The touchscreen trainings and tasks are summarized in Suppl. Table 5. Mice were 65-69 weeks old at the onset of the touchscreen training.

## Touchscreen – 5-choice serial reaction time (5-CSRT)

One week prior to the habituation phase, mice were set on a restriction diet with 2–3 g of food pellets per day to reduce the body weight to 90 %. The diet was maintained throughout experiments to increase the appetite for the liquid reward, which consisted in 8 µl sweetened condensed milk (Nestlé, Switzerland; diluted 1:4 in tap water). For stimulus presentation within the 5CSRT task, a black Perspex mask with five windows was placed in front of the touchscreen. The training steps were adapted from the procedures published by the Bussey and Holmes laboratories(46),(47). During the training stages, the animals learned to touch the screen in correct locations to get a tone-coupled reward. In the "Must-Touch" training, the mouse had to touch the screen at any site in response to the stimulus to collect the reward. In the next "Must Initiate" training, the mouse had to trigger the stimulus by poking into the illuminated reward through. The trigger-to-stimulus delay was 5 s. The criterion of success was defined by a completion of 30 trials within 60 min on two consecutive training days. For the 5CSRT task, a white-square is presented pseudo-randomly in one out of five possible locations, and the mouse has to touch the screen in the correct position. Outside of the lit rectangle, the screen is dark. In the "Punish Incorrect" training, settings were as in Must Initiate but a timeout period of 5 s was triggered if the mouse touched the blank site of the screen outside of the enlightened square. During timeout, the image disappeared and the overhead lighting (~60 Lux) was turned on for 5 s. The criterion was to complete 30 trials in 60 min with > 65 % correct responses. The criterion of success was not met by sufficient animals so that the 5CSRT testing phase in which the time stimulus presentation is progressively reduced was not reached. The 5CSRT task primarily addresses attention, responses to short visual stimuli, spatial discrimination and impulse control.

## Touchscreen - Pairwise Discrimination (PwD) and Reversal

The Pairwise Discrimination & Reversal tasks were done after completion of the 5-CSRT. For stimulus presentation, a black perspex mask with two windows was placed in front of the touch screen. During training stages, a white simple pictogram of an object on black background

(Campden/Lafayette software) was presented in one of the two windows. The mice had to touch the pictogram-window in order to elicit a tone-coupled reward. During test sessions, two novel stimuli (pictograms) were presented in a spatially pseudo randomized order over 30-trial sessions (20 s intertrial-interval, ITI) in the absence of overhead lighting. One image was set to correct, the other to incorrect. Responses to the correct stimulus resulted in 8 µl reward. Responses to the incorrect stimulus resulted in a 5 s timeout, coupled with switching the ~60 lux house light on. This was followed by a correction trial. Stimuli remained on the screen until a response was made(48),(49). The criterion to enter the reversal stage was to complete 30 trials in 60 min with >65 % correct responses, for a minimum of 3 consecutive testing days. During the reversal stage, the previous correct image was set to incorrect and coupled with overhead lighting for 5 s. Inversely the previous unrewarded image was set to correct and elicited the tone-coupled reward supply. The criterion for reversal learning was an average percent correctness of 80 % or higher. The performance in the PD task involves functioning of glutamatergic and muscarinic systems[48],[50],[51].

# Results

## Expression of EGFL7 in the HC of mice and man

To visualize the expression and localization of EGFL7 in the HC, we analyzed human specimens by immunofluorescence (**Fig. 1a**) and immunoperoxidase staining (**Supplementary Fig. 1a).** Neurons of the DG and the hilus of human HCs stained strongly positive for EGFL7 (**Fig. 1a, Supplementary Fig. 1a**). Specimens of human placenta served as a positive control(52) which readily expressed human EGFL7 in trophoblast cells (**Supplementary Fig. 1b,c).**

Furthermore, the expression of murine EGFL7 in mouse specimens was analyzed by FISH, which revealed a clear expression of EGFL7 throughout the DG of adult mice (**Fig. 1b, right panel**). No signal was detected in the DG of *EGFL7*-/- mice (**Fig. 1b, left panel**), thus verifying probe specificity.

To identify the cellular origins of EGFL7 in the HC, tissues were minced and cells of the DG separated by fluorescence-activated cell sorting. Such sorted cells were analyzed by qRT-PCR, which revealed a ubiquitous transcription of *Egfl7* with substantial differences in transcript abundance between cell types (**Fig. 1c**). High levels of *Egfl7* were synthesized in neurons (17.2 ± 0.16-fold enriched as compared to unsorted HC tissue), NPCs (41.4 ± 0.21-fold), quiescent qNSCs (46.7 ± 0.37-fold) and activated aNSCs (132.7 ± 1.50-fold). The latter cells displayed highest expression levels with close to a 3-fold increase as compared to qNSCs. Smaller amounts of *Egfl7* were detected in neuroblasts (NBs; 3.0 ± 0.11-fold increase). *Egfl7* transcription was visualized *in situ* by a combination of *Egfl7*-specific FISH probes and cell-specific IF markers. This way *Egfl7* was predominantly identified in Stathmin(Stmn1$^{+}$)-positive aNSCs/NPCs and NeuN$^{+}$ neurons (**Fig. 1d**).

In conclusion, EGFL7 is majorly expressed in neurons as well as proliferating stem and progenitor cells in the DG of the HC.

## Loss-of-EGFL7 promotes the proliferation of NSCs

A functional impact of EGFL7 on NSCs/NPCs *in vitro* was assessed in HC-derived neurospheres of *EGFL7-/-* mice as compared to wild-type (WT) littermates. Spheres of *EGFL7-/-* mice grew larger in diameter (58.95 ± 11.24 µm versus 43.85 ± 2.25 µm in WT; **Fig. 2a,b**), suggesting an increased proliferation rate of aNSCs/NPCs upon EGFL7 KO, which may be due to enhanced NSC activation or sustained proliferation. A cell cycle analysis of isolated NSCs revealed that the deletion of EGFL7 diminished the amount of cells in G1 phase but led to a concomitant increase of cells in G2/M phase (**Fig. 2c**), pointing towards an increased activation rate of qNSCs. In order to test this hypothesis, we subjected NSCs isolated from the HC of *EGFL7-/-* mice and WT to flow cytometry analyses using three cell markers ($GLAST^+/CD133^+/EGFR^{-/+}$) to discriminate between qNSCs and aNSCs (**Supplementary Fig. 2**). A significantly higher amount of aNSCs was isolated from the DG of *EGFL7-/-* mice (5.6 ± 1.65%) as compared to WT (2.2 ± 0.53%), verifying a higher frequency of cell cycle entry of qNSCs *in vivo* (**Fig. 2d**). This suggests that either phases of quiescence of qNSCs were shorter upon KO or proliferation of NSCs became triggered by pro-mitotic cues.

The amount of proliferating cells in the HC at different time points was visualized *in vivo* upon intraperitoneal application of two different thymidine analogues, namely IdU and CldU. Both markers are incorporated into the DNA of proliferating cells only. IdU was injected 24 h before and CIdU 1 h before subjects were sacrificed in order to discriminate among cells just entering S phase ($CldU^+$; **Fig. 2e,f**) or continuously proliferating after 24 h ($Ki67^+/IdU^+$; **Fig. 2e,g**). Twice the amount of proliferating cells was detected in the SGZ of *EGFL7-/-* mice as compared to WT at both time points, which supports the conclusion that the pool of proliferating cells in the HC becomes sustainably enhanced in adult mice upon EGFL7 deletion.

## EGFL7 deletion stimulates neurogenesis in the HC by expansion of type 2a progenitors

To determine the influence of EGFL7 on adult neurogenesis in the HC *in vivo*, NSCs and their progeny were quantified in constitutive *EGFL7-/-* mice and WT combining cell-specific IF markers (**Fig. 3a**) with

the thymidine analog BrdU to permanently label proliferating cells and their descendants. Mice were housed in cages with an enriched environment (EE) and access to wheels allowing for voluntary running in order to stimulate neurogenesis(53). Mice were sacrificed 3 d and 28 d after administration of BrdU in order to examine either early stages (represented by aNSCs, NPCs, NBs) or later stages (represented by immature and mature neurons) of neurogenesis (**Fig. 3b**).

The amount of proliferating GFAP$^+$/Nestin$^+$/BrdU$^+$ RGL type 1 stem cells was found to be approximately equal among *EGFL7*-/- mice and WT litters *in vivo* (**Fig. 3c**). Mash1$^+$/BrdU$^+$ type 2a progenitors were increased by about 2-fold (**Fig. 3d**) and DCX$^+$/BrdU$^+$ type 2b progenitors were found to be decreased by about 2-fold (**Fig. 3e**). The Stmn1$^+$/BrdU$^+$ positive population represents all proliferating progenitor cells, including aNSCs/NPCs and type 3 progenitors - already committed towards neuronal differentiation - and was found increased by about 3.5-fold upon deletion of EGFL7 (**Fig. 3f**). Interestingly, different subtypes of cells within this heterogeneous proliferating cell population were affected in an opposing manner by the loss-of-EGFL7.

In order to understand the overall increase in the Stmn1$^+$/BrdU$^+$ positive population, sections were stained for Ki67/DCX or DCX/NeuN in order to discriminate between proliferating and post-mitotic NBs/immature neurons by IF. Mitotically active type 2b and type 3 progenitor cells (Ki67$^+$/DCX$^+$) were reduced in number (**Supplementary Fig. 3a**)while the amount of immature neurons (DCX$^+$/NeuN$^+$) was increased in *EGFL7*-/- mice as compared to WT litters (**Supplementary Fig. 3b**). The number of adult born mature neurons, quantified as NeuN$^+$/BrdU$^+$ cells, was 4-fold increased (**Fig. 3g**).

These results lead to the conclusion that the constitutive deletion of EGFL7 stimulated neurogenesis in the HC principally by the expansion of the type 2a progenitor cell pool. Given this fact, deletion of EGFL7 in progenitors should phenocopy the above observations. Therefore, *EGFL7 fl/fl;Ascl1-CreERT2*, a tamoxifen-inducible cell-type specific EGFL7 KO system based on the expression of *Ascl1-CreERT2*, was applied allowing for the conditional deletion of EGFL7 in mostly type 2a progenitors (**Fig. 4a**). The experimental setup was comparable to the preceding experiment with the only difference that mice received three injections of tamoxifen ip at 8 weeks of age (**Fig. 4b**). Indeed,

type 2a-specific deletion of EGFL7 yielded comparable results to those collected in constitutive *EGFL7*-/- mice (**Fig. 3**). Type 2a progenitors (**Fig. 4c**) and $Stmn1^+/BrdU^+$ positive population (**Fig. 4e**) were increased, type 2b/3 progenitors were reduced (**Fig. 4d**) but in particular the amount of newborn neurons was significantly increased in *EGFL7 fl/fl;Ascl1-CreERT2* mice (18.25 ± 6.80 versus 5.50 ± 2.65 cells per section in WT; **Fig. 4f**).

In conclusion, the increase of adult hippocampal neurogenesis upon EGFL7 KO is majorly mediated by type 2a progenitor cells.

In order to verify cell-type specificity of the decrease in $DCX^+/BrdU^+$ type 2b progenitors in constitutive *EGFL7*-/- mice (**Fig. 3e**), *EGFL7 fl/fl;DCX-CreERT2* mice were analyzed (**Supplementary Fig. 4a,b**). In this model EGFL7 is deleted from type 2b/type 3 cells and post-mitotic neuroblasts upon TAM induction. The amount of type 2a cells remained uneffected (**Supplementary Fig. 4c**) but a significant reduction of $DCX^+/BrdU^+$ type 2b and $Stmn1^+/BrdU^+$ progenitors was observed (**Supplementary Fig. 4d,e**) upon *Egfl7* deletion. However, in the absence of type 2a cell expansion, the number of adult-born $NeuN^+/BrdU^+$ double positive neurons was reduced (**Supplementary Fig. 4f**).

Data strongly suggest that the increase of adult-born neurons in constitutive *EGFL7*-/- mice is mainly caused by the increase in proliferating type 2a progenitor cells upon EGFL7 deletion.

## EGFL7 regulates neurogenesis by cytokine VEGF-D

The data above suggested that EGFL7 expanded the type 2a cell pool in the SGZ of the HC in order to stimulate neurogenesis. However, the molecular mechanism EGFL7 engaged to trigger this phenotype remained enigmatic. Therefore, RNA sequencing experiments on aNSCs/NPCs derived from *EGFL7*-/- mice and WT controls were performed (**Fig. 5a,b**). This particular experiment consisted of two sequential studies. Comparisons of regulated gene sets I) confirmed the deletion of EGFL7, II) revealed a reciprocal expression of VEGF-D (Venn diagrams) and III) identified additional top regulated candidates (**Supplementary Fig. 5)**. Transcriptomic results on VEGF-D were confirmed by

qRT-PCR, which exhibited a 6-fold increase of VEGF-D in *EGFL7*-/- aNSCs/NPCs as compared to WT (**Fig. 5c**). IF studies of VEGF-D *in vivo* showed higher numbers of VEGF-D-positive cells in the DG of *EGFL7*-/- mice as compared to WT (**Fig. 5d**), pointing towards a so far unrecognized role of VEGF-D in hippocampal neurogenesis.

In order to assess the functional relevance of VEGF-D in the HC, recombinant purified protein was infused via osmotic pumps into the ventricle of 8-week-old WT mice for 7 d (**Fig. 6a**). In parallel, proliferating cells were labeled *in vivo* by administration of the base analogs IdU and CldU ip at d1 and d6, respectively (**Fig. 6b**). At d7 animals were sacrificed by transcardial perfusion, brains were removed, fixed, and HCs sliced in order to characterize NSCs and their progeny by IF analyses as described above. Stainings revealed a significant increase in $CldU^+$ cells upon the administration of recombinant VEGF-D (**Fig. 6c**). In particular, the number of type 2a cells ($Mash1^+/CldU^+$) was elevated 2-fold (**Fig. 6d**). Further, the amount of aNSCs/NPCs ($Stmn1^+/CldU^+$) was increased 3-fold (**Fig. 6e**). Additionally, the amount of adult-born immature neurons ($DCX^+/NeuN^+$) increased upon the administration of VEGF-D for one week (**Fig. 6f**).

These data support the conclusion that VEGF-D stimulates neurogenesis in the HC and EGFL7 exerts its function via this cytokine.

## Notch signaling in HC-derived aNSCs/NPCs

EGFL7 has been identified as a non-canonical Notch ligand that affects Notch signalling *in vivo* and *in vitro*(26),(27). To define potential candidates responsible for differential effects of EGFL7 on NSCs and their progeny in the HC, Notch signalling components were quantified by qRT-PCR in HC-derived aNSCs/NPCs (**Supplementary Fig. 6**). Prominent levels of the Notch receptors 1-3, the neuron-specific Delta/Notch-like EGF-related receptor (DNER), the canonical ligand Jagged1, the non-canonical ligands Dlk2,Dll3 and Dll4 as well as the Notch reporter genes Hes1, Hes5, Hey1 and Hey2 were detected (**Supplementary Fig. 6a,b**). On the contrary, the expression levels of Notch4, Dll1, Jagged2,

Dlk1 and Hes3 were smaller than 0.05 as normalized to EGFL7 and were therefore not included in the diagram. Last, relevant expression levels of lunatic fringe (LNFG), manic fringe (MFNG) and radical fringe (RFNG), modifiers of Notch receptor fucosylation, were spotted in HC-derived aNSCs/NPCs (**Supplementary Fig. 6a,b**). However, no significant differences in the expression levels of either Notch component were detected upon deletion of EGFL7, suggesting that EGFL7 exerts its function in HC-derived aNSCs/NPCs not to a significant extend via Notch.

## EGFL7 affects spine formation and longterm survival of adult-born DG neurons

Adult-born neurons do not necessarily integrate into the existing neural network. As a matter of fact most of them do not survive for a long time(8). This prompted the question whether the additional adult-born neurons generated upon EGFL7 deletion integrate into the DG network and persist or if they fade away. As VEGF-D has been reported to modulate dendrite complexity in the adult mouse hippocampus(54), spines of mature hippocampal neurons were classified upon EGFL7 KO *in vivo* using the *Thy1-GFP*-M1 model (**Fig. 7**). For this purpose, *Thy1-GFP* mice were crossed with *EGFL7-/-* mice which allowed for a comparison between dendritic spines on neurons of the HC (now labeled with GFP) in *EGFL7-/-* animals and WT litters. Neurons of the DG in *EGFL7-/-;Thy1-GFP* mice displayed higher spine density as compared to WT control at 10 weeks of age (**Fig. 7a-c**). In particular, the population of thin spines, described as learning spines(55), was found increased upon EGFL7 deletion (**Fig. 7c**). This difference faded away at 20 weeks of age (**Fig. 7d-f**), suggesting that it is a phenotype of young rather than mature neurons. For this reason the model is suitable for the analysis of events occurring on immature adult-born neurons in the DG. To further assess if these effects are specific to DG neurons, other areas of the HC have been analyzed in the context of dendritic complexity. Analysis of dendritic spines of the CA1 region of the HC revealed no difference in spine number or morphology upon the loss of EGFL7 (**Supplementary Fig. 7a-c**).

Additionally, the dendritic outgrowth of neurons in primary neuronal cultures of newborn mice (P1) was examined. Quantitative analysis showed a significant increase in dendrite number and total

dendritic length of Map2 positive neurons isolated from *EGFL7*-/- mice as compared to WT litters (**Fig. 7g,h).**

Data allow for the conclusion that the deletion of EGFL7 led to an increase in thin spines on young neurons, such supporting their neural network integration and survival of adult-born neurons in the DG. In order to test this young mice received one injection of BrdU and were sacrificed at the age of 9, 50 or 75 weeks (**Fig. 7i**). Quantification of $BrdU^+/NeuN^+$ double positive neurons revealed an increase in adult-born neurons in young mice upon the loss of EGFL7, which persisted until old age (**Fig. 7i**). Due to the longterm survival of these additional aduld-born neurons *EGFL7*-/- mice may display cognitive differences in comparison to their WT litters.

## EGFL7 deficiency improved spatial memory in young mice

Findings above raised the question whether the EGFL7-mediated orchestration of adult neurogenesis is of physiological relevance for living animals, which prompted us to assess learning and memory in behaving mice. In the MWM both groups showed equivalent swimming velocity and times to reach the visible platform (**Fig. 8a**), which is a prerequisite for interpretation of spatial learning. Body weights were comparable throughout experiments (exemplary cohort **Fig. 8b**). As a result, *EGFL7*-/- mice reached the hidden platform of the MWM faster than their WT litters (**Fig. 8c**), which was evident by comparing AUCs and time courses. Genotype differences manifested in the late trials suggesting a stronger memory consolidation and possibly, stronger stimulating effect of daily swimming exercise. Indeed, *EGFL7*-/- mice retained stronger preference of the target quarter after removal of the platform (**Fig. 8d**). The Morris water maze is influenced by the swimming dislike of mice and therefore, further spatial tests were done using a Barnes maze (**Supplementary Fig. 8_1**). There was no difference in the classical test requiring escape through one target hole into the escape box, neither during acquisition nor during reversal (**Supplementary Fig. 8_1a**), but in a 2-choice award-based paradigm, *EGFL7*-/- mice were faster to escape (**Supplementary Fig. 8_1b**).

Based on these results, specific tests were designed in the IntelliCage which provides a PC-controlled observation of groups of mice without handling. In the first set of experiments, mice were 10-16 weeks old at the start of the observations, in the range of ages used for MWM. In these young adults, the overall activity of visits, nosepokes and licks was very similar in both genotypes throughout the observation period lasting up to midlife (**Supplementary Fig. 8_2a**). There was also no difference in the acquisition of avoidance (**Fig. 8e**) or corner preferences (**Fig. 8f**). However, *EGFL7*-/- mice retained longer memory of a previously "punished" forbidden corner as indicated by lower errors (**Fig. 8e**), and they were faster to re-establish preference of a rewarded corner after its removal to the opposite side of the cage (**Fig. 8f**). This reversal learning period is the most critical and most difficult part and suggested a crucial advantage of *EGFL7*-/- mice over their WT litters. Further analysis of the periods outside of the learning modules, in which the doors remained closed, revealed that *EGFL7*-/- mice retained stronger corner preference without re-enforcement (**Fig. 8 g,h**), which agrees with the maze experiments and suggests that EGFL7 deficiency strengthens spatial memory.

The cohort of mice of Figure 8 returned to the IntelliCage at middle age (57-60 weeks at start). In the meanwhile, they had spent a normal mouse life without experiments *EGFL7*-/- showed higher activity than the controls (**Supplementary Fig. 8_2b**). Activity in the IC drops during aging(41), and the activity of the *EGFL7*-/- was closer to the activity of the young. To further address learning & memory in visual spatial paradigms, these mice were subjected to Touchscreen observations.

## No genotype differences in old mice in Touchscreen tasks

*EGFL7*-/- mice and their WT litters were observed in touchscreen learning chambers subsequent to experiments in the IntelliCage. They were 63-69 weeks at start and 74-80 weeks old at completion. They performed the 5-CSRT and Pairwise Discrimination and Reversal tasks as detailed in Methods and Suppl. Tables. In the 5-CSRT (**Supplementary Fig. 8_3a**), which measures attention and response velocity, both genotypes reached the Punish Incorrect (PI) training phase, in which the time of presentation of the bright rectangle is not yet limited, but both genotypes did not pass this training

level owing to their old age. The success criterion was set at 75% accuracy in PI. During Must Touch and Punish Incorrect, there were no differences in touch latencies, reward collection latencies or percentage of correct trials between genotypes.

Subsequent to 5-CSRT, mice were tested in the Pairwise Discrimination and Reversal Task (**Supplementary Fig. 8_3b**), which requires discrimination and learning of visual objects and is sensitive to cholinergic signaling(56),(57). Neither accuracy nor latencies for screen touch or reward collection differed between genotypes. Half of the mice in each group passed the criterion of success in the learning phase and moved on to the Reversal learning. Accuracy dropped in both genotypes during Reversal and returned to the previous learning level after 5-6 trial days. The time courses (**Supplemenatry Fig. 8_3c**) were similar in both genotypes. During all touchscreen experiments mice were kept under a 10% restriction diet to increase the motivation for the sweet-milk reward. The body weight loss was equivalent in both groups (**Supplementary Fig. 8_3d**) suggesting equal reward appeal.

**High activity in old EGFL7-deficient mice**

The touchscreen experiments did not reveal cognitive advantages or disadvantages of EGFL7-/- at old age. However, the overactivity observed in aged mice (**Supplementary Fig. 8_2**) is an indicator of age-associated behavioral differences. To address this question behavior in the IntelliCage was analyzed in a second cohort of old EGFL7-deficient and control mice. Mice were 82-88 weeks old at the start or IC observations. *EGFL7fl/fl;EIIa-Cre and EGFL7fl/fl* control litters were used to address putative effects of genetic constructs. As expected *EGFL7fl/fl;EIIa-Cre* mice were overactive throughout the observations, but predominantly during the non-learning adaptation periods where the corner visiting activity reflects exploration and curiosity (**Fig. 9a,c**). Hyperactivity manifested predominantly in SVisits (**Figure 9a, second row**), which are exploratory Visits without Licks or NPs, i.e., without drinking purpose. Visits with licking purpose (LVisits) were less affected (**Figure 9a, first row**). Exploratory SVisits are high in young mice and at onset of IntelliCage experiments, whereas

aged to old mice mainly visit the corners for drinking purposes (LVisits)(41)'(58)'(59). High exploration in young mice is associated with a relative high frequency of errors(41) which was not the case in *EGFL7fl/fl;EIIa-Cre* animals (**Fig. 9b**). Indeed, SVisits dropped during the place preference learning periods (grey shaded), particularly when mice were exposed to mild daily circadian stressors referred to a CUMS (chronic unpredictable mild stress), and the accuracy of nosepokes was slightly higher in *EGFL7fl/fl;EIIa-Cre* mice compared with the controls (**Fig. 9b**). Hence, the visiting activity was high, but the mice did not make try-and-error NPs, suggesting that they were curious and active like young mice but still attentive. Paired analysis of the trials and errors and the accuracy (percentage of correct trials) clearly revealed an overactivity (**Fig. 9c**) but no differences in accuracy between genotypes. Data suggest that EGFL7-deficient mice retained an active youthful life at old age and displayed no cognitive disadvantages.

## Discussion

The neurogenic niche in the HC is located deep within the DG of the hippocampal parenchyma and is majorly formed by neurons, neural precursor cells, astrocytes(60), blood vessels(61) and the extracellular matrix (ECM). The cells in this network are connected by nerve fibres allowing NSCs and adult-born neurons to respond to neural activity in the HC(62). In parallel, these cells are governed by ECM modulation or secreted factors acting in a paracrine or endocrine fashion(62).

The local microenvironment significantly differs between the two neurogenic niches in the mammalian brain. NSCs of the SGZ (termed type 1 cells) and SVZ (termed B cells) display astroglial properties and are derived of RGLs in the subventricular zone of the developing brain(63). This descendance is reflected by a characteristic morphology with a long apical process, which in case of type 1 cells extends through the GC layer(64) and branches in the inner molecular layer of the HC(65). Type 1 cell processes form tight appositions with axon terminals and spines, similar to astrocytes but importantly, they do not establish synaptic contacts(65). Basal processes project along the SGZ axis into the hilus where they receive input of hilar neurons(65). In the SGZ, NSCs contact not only nearby neurons of the GC layer but also local interneurons and mossy cells, thus forming a neural network governing local neurogenesis(62). This is in contrast to NSCs in the SVZ, which lack contact to a larger amount of neurons but instead are located close to blood vessels and the lateral ventricles(66).

Another difference between these neurogenic niches is the process of neurogenesis itself. Neuroblasts of the SVZ migrate about 5 mm in mice(67, 68) before they reach the OB, differentiate into inhibitory interneurons and connect to the olfactory microcircuit. These adult-born periglomerular (5%) or granular (95%) interneurons participate in neural circuits of olfaction(69). In contrast, adult-born neurons and their progeny in the SGZ stay mostly local and connect with long axons to GCs of the CA3 region of the HC. Their apical dendrites reach into the molecular layer of the HC and form a characteristic dendritic tree allowing them to receive input from the entorhinal cortex via the performant path(70). Together, these differences point towards a significant distinction

between the adult neurogenesis processes in the SGZ and the SVZ as well as their regulatory mechanisms.

Furthermore, the amount of adult-born neurons in the two neurogenic regions significantly differs. While the SVZ in adult rats gives rise to about 30,000 neurons a day, only a few 1,000 are produced by the SGZ(71). Even less are formed in the human SGZ (only about 700 a day)(8). Surprisingly, adult-born neurons were detected in tissue samples of almost 90-year-olds(72), suggesting that adult neurogenesis occurs in the human DG throughout life. However, it was not spotted in the human OB(73). One may conclude from this fact that hippocampal neurogenesis is of greater relevance for humans because of its impact on learning and memory(74) while smell is more relevant for rodents.

Previously, we have described EGFL7 as a factor altering the microenvironment, shaping the regulation of NSCs in the SVZ and governing adult neurogenesis in the OB. Loss-of-EGFL7 led to an accumulation of aNSCs/NPCs in the SVZ and pushed neuronal progeny towards differentiation by promoting Dll4-induced Notch signalling in the neurovascular stem cell niche. In this way, increased neurogenesis caused an imbalance in the number of excitatory and inhibitory neurons in the OB, leading to a desynchronization of the olfactory network, which manifested in a disturbed olfactory perception of *EGFL7*-/- mice(27).

In this work, the role of EGFL7 for NSC regulation in the SGZ and its relevance for adult neurogenesis in the DG was studied. In the human HC, EGFL7 was majorly detected in neurons, in particular in GCs of the DG and in hilar neurons. Furthermore, endothelial cells of larger blood vessels displayed immunoreactivity as expected(29). Expression studies in mice using FISH confirmed the expression of EGFL7 in GCs and revealed that NSCs/NPCs as well as neurons synthesized the majority of EGFL7 in the SGZ.

In order to test if EGFL7 affected NSC proliferation in the SGZ, NSCs were isolated from the DG of *EGFL7*-/- and WT litters and were grown as neurospheres *in vitro*. *EGFL7*-/- spheres grew much larger suggesting increased cell proliferation. This finding was verified *in vivo* by flow cytometry analysis, which identified double the amount of aNSCs in the DG of *EGFL7*-/- mice as compared to WT litters.

Furthermore, this increased amount of proliferating progenitors was confirmed by IF analyses, which allows for the conclusion that aNSCs/NPCs increasingly proliferated in the absence of EGFL7 raising questions regarding the molecular mechanism governing this phenotype.

Previously, Notch has been identified as a major regulator of NSCs in the SGZ(23) and EGFL7 has been shown to modulate this interface(26),(27). Notch signalling strongly influenced neurogenesis in the SGZ of the DG in mice(75),(76). Induced Notch-deficiency resulted in an abolition of neurogenesis by a loss-of-NSCs and a reduction in mitotic progenitors. Eventually, loss of Notch1 caused a depletion of the NSC population in the SGZ(77). Conversely, activation of Notch1 increased the NSC population and generated a higher number of glial cells at the expense of neurons(75).

In comparison, loss-of-EGFL7 caused an upregulation of neurogenesis in the SGZ and an increase in aNSCs/NPCs as well as a decrease in neuroblasts, but the stem cell pool remained unaffected. Partially, these observations supported the idea that EGFL7 may affect NSC proliferation in the SGZ via Notch. However, differences between the Notch and EGFL7 phenotype were striking and loss of EGFL7 did not affect Notch signalling in HC-derived aNSCs/NPCs to a significant extend. This suggested the engagement of alternative signalling pathways by EGFL7 beyond Notch.

Transcriptomics of NSCs revealed an upregulation of VEGF-D upon EGFL7 KO. This particular cytokine is produced among other cell types by neurons in the adult brain(54). NSCs in the DG have been shown to express VEGF-D's receptor VEGFR-3, a receptor tyrosine kinase activating the AKT and ERK pathways upon ligand binding and thereby controlling cell fate and proliferation(78). This suggested that the aNSC/NPC pool in *EGFL7-/-* mice was expanded by the upregulation of VEGF-D. In order to test this, purified recombinant VEGF-D was infused in the DG by osmotic pumps for a period of seven days. Indeed, infusion of VEGF-D phenocopied the effect seen in the EGFL7 KO in this time frame indicating that VEGF-D acted downstream of EGFL7. Interestingly, VEGF-D has been described to support dendritic and synaptic plasticity as evoked by exercise(79). Moreover, VEGF-D preserved the dendritic architecture and facilitated functional recovery in a murine model of stroke(54)

strengthening the hypothesis that VEGF-D and EGFL7 together orchestrate neurogenesis in the adult HC.

Spine number and plasticity are tightly associated with synaptic function in the mammalian brain(80, 81). The relationship between spine formation and synaptic activity is best characterized in the apical dendrites of pyramidal neurons in the hippocampal CA1 subfield(82), but the dentate gyrus is the predominant point of synaptic entry, and is crucial for episodic memory formation and pattern separation(83, 84). Dentate granule cells differ from CA1 pyramidal neurons in terms of their morphology and biophysical properties(82). The loss of EGFL7 was associated with an increase of spine density of the granule cells, but not of CA1 neurons.

Maintenance of neurogenesis and spine plasticity in the adult hippocampus are both believed to preserve cognitive youthfulness and have been suggested as a path towards healthy aging(54, 85, 86). In support of this hypothesis, exercise improves learning, memory, and longevity(87-89). Furthermore, the overexpression of pro-neurogenic factors in mice restored spine loss and cognitive deficits in some models of dementia(90, 91). In line with these assumptions, *EGFL7*-/- mice displayed subtle but distinct and reproducible advantages in a number of reward- and avoidance-based memory tasks in young adult mice. The predominant phenotype in various different behavioural studies was a stronger maintenance of memory. This manifested in 1) shorter paths towards platform or rewarding box in late training trials in the Morris water maze and 2-choice Barnes maze, 2) stronger maintenance of platform quarter preference after removal of the platform, 3) longer avoidance of air puff-punished corners and 4) stronger adherence to preferred corners in non-rewarded periods in the IntelliCage. Taken together, these tests point towards a longer-lasting spatial memory and an improved memory consolidation in *EGFL7*-/- mice, parameters affected by adult neurogenesis in the HC by the modulation of pattern separation(79, 92-94). In addition, *EGFL7*-/- mice were faster in reversal learning, which is the most critical and most difficult part in learning tasks, because it requires a switch of strategy and search for alternative solutions. In fact, this type of cognitive flexibility is majorly mediated by the HC(19, 95, 96). Taken together, these tests point

towards a longer-lasting spatial memory and an improved memory consolidation in *EGFL7*-/- mice, parameters affected by adult neurogenesis in the HC by the modulation of pattern separation(92)[,(93),(79),(94)]. In addition, *EGFL7*-/- mice were faster in reversal learning, which is the most critical and most difficult part in learning tasks, because it requires a switch of strategy and search for alternative solutions. In fact, this type of cognitive flexibility is majorly mediated by the HC[(19),(95),(96)].

The overall activity of young adult mice was equal in both genotypes. However, while the control mice showed the normal age-dependent loss of activity, EGFL7 deficient mice retained high activity like young mice. This was not associated with a loss of accuracy, which characteristically occurs in models of dementia or post traumatic brain injury[(42),(97)]. In these models, hyperactivity is associated with a high frequency of errors injury[(42),(97)]. In contrast, EGFL7 deficient mice were mainly hyperactive in adaptation periods, but not so much so in preference learning periods when attention and memory was required to get reward. Hence, the overactivity of aged and old EGFL7 mice can be interpreted as youthful curiosity and exploration and is not indicative of dementia-like behaviour. The interpretation is supported by the performance in Touchscreen tasks of old EGFL7 deficient mice, which was equal to the controls. Hence, the behavioural studies suggested that EGFL7-deficiency mediated was associated with an enhancement of some cognitive capabilities in young adult mice, which is not maintained up to old age but leads to a more active exploratory phenotype reminiscent of the playful activity of young mice. Translated to human, the EGFL7-deficient old would behave like the 30-year old but would be able to focus if required.

However, it remains enigmatic how the loss of a gene may improve learning and memory and in fact, *Egfl7* is an unusual and rare case. It seems counterintuitive because smarter mice should have an evolutionary advantage over their litters expressing EGFL7. In consequence, one would expect that this gene was counter-selected in evolution and silenced but this was not the case. One may conclude that EGFL7 inherits functions beyond intelligence and more relevant for mice. For instance, mice explore their environment to a significant extent by smelling; therefore, their OB accounts for 2% of the brain as compared to 0.01% in humans(98). However, *EGFL7*-/- mice displayed significant

olfactory deficits and did not react to an extract of fox urine(27). In the wild, these animals would become easy prey for predators and a counter-selection of *Egfl7* did therefore not occur in evolution. Immediately, this raises the question of the role of EGFL7 in the human brain. Our survival does not rely on olfactory cues to a significant extent, but significant amounts of EGFL7 were still detected in the human HC. Due to its influence on learning and memory, we may be able to improve these processes by blocking EGFL7 function in the HC. Alternatively, the cytokine VEGF-D could be administered in order to phenocopy the EGFL7 KO, which seems technically more feasible. Either way, an increase in learning and memory may be achieved, in particular in old age when cerebral fitness becomes limited. Such an improvement in mental capacity in our steadily aging society may help people to grow in age with reduced memory loss.

## Author contributions

VV and KB performed experiments, analysed data and wrote the manuscript; FB, CM, NH, CR, UN, LS, MM and KR performed experiments and analysed the data; US, JB, TM, ST and FZ analysed data and contributed to writing of the manuscript; IT and MHHS designed the study and wrote the manuscript.

## Acknowledgements

We thank Martin Adrian, Nicole Feind, Anja Motz, Anja Neißer, Martina Pinkert, Kerstin Pehlke, Doreen Streichert and Alexander Wenzel for excellent technical assistance as well as Cheryl Ernest for proofreading the manuscript. This work was supported by the German Research Foundation (DFG) via the collaborative research centres 1080, projects A03 (IT & MHHS), C01 (FZ), C02 (IT & TM) and 1292, projects TP09 (MHHS & FZ), Z01 (ST) as well as the DFG grant SCHM 2159/4-1 to MHHS.

## Conflict of interest

The authors declare that they have no conflicts of interest.

Supplementary information is available at MP`website.

## References


1. Seki T, Arai Y (1999): Temporal and spacial relationships between PSA-NCAM-expressing, newly generated granule cells, and radial glia-like cells in the adult dentate gyrus. *J Comp Neurol*. 410:503-513.
2. Barnea A, Nottebohm F (1994): Seasonal recruitment of hippocampal neurons in adult free-ranging black-capped chickadees. *Proc Natl Acad Sci U S A*. 91:11217-11221.
3. Kuhn HG, Dickinson-Anson H, Gage FH (1996): Neurogenesis in the dentate gyrus of the adult rat: age-related decrease of neuronal progenitor proliferation. *J Neurosci*. 16:2027-2033.
4. Kempermann G, Kuhn HG, Gage FH (1997): More hippocampal neurons in adult mice living in an enriched environment. *Nature*. 386:493-495.
5. Eriksson PS, Perfilieva E, Bjork-Eriksson T, Alborn AM, Nordborg C, Peterson DA, et al. (1998): Neurogenesis in the adult human hippocampus. *Nat Med*. 4:1313-1317.
6. Roy NS, Wang S, Jiang L, Kang J, Benraiss A, Harrison-Restelli C, et al. (2000): In vitro neurogenesis by progenitor cells isolated from the adult human hippocampus. *Nat Med*. 6:271-277.
7. Knoth R, Singec I, Ditter M, Pantazis G, Capetian P, Meyer RP, et al. (2010): Murine features of neurogenesis in the human hippocampus across the lifespan from 0 to 100 years. *PLoS One*. 5:e8809.
8. Spalding KL, Bergmann O, Alkass K, Bernard S, Salehpour M, Huttner HB, et al. (2013): Dynamics of hippocampal neurogenesis in adult humans. *Cell*. 153:1219-1227.
9. Boldrini M, Fulmore CA, Tartt AN, Simeon LR, Pavlova I, Poposka V, et al. (2018): Human Hippocampal Neurogenesis Persists throughout Aging. *Cell Stem Cell*. 22:589-599 e585.
10. Ming GL, Song H (2011): Adult neurogenesis in the mammalian brain: significant answers and significant questions. *Neuron*. 70:687-702.
11. Kang E, Wen Z, Song H, Christian KM, Ming GL (2016): Adult Neurogenesis and Psychiatric Disorders. *Cold Spring Harb Perspect Biol*. 8.
12. Anacker C, Hen R (2017): Adult hippocampal neurogenesis and cognitive flexibility - linking memory and mood. *Nat Rev Neurosci*. 18:335-346.
13. Kempermann G, Gage FH, Aigner L, Song H, Curtis MA, Thuret S, et al. (2018): Human Adult Neurogenesis: Evidence and Remaining Questions. *Cell Stem Cell*. 23:25-30.
14. Berdugo-Vega G, Arias-Gil G, Lopez-Fernandez A, Artegiani B, Wasielewska JM, Lee CC, et al. (2020): Increasing neurogenesis refines hippocampal activity rejuvenating navigational learning strategies and contextual memory throughout life. *Nat Commun*. 11:135.
15. Goncalves JT, Schafer ST, Gage FH (2016): Adult Neurogenesis in the Hippocampus: From Stem Cells to Behavior. *Cell*. 167:897-914.
16. Kempermann G, Jessberger S, Steiner B, Kronenberg G (2004): Milestones of neuronal development in the adult hippocampus. *Trends Neurosci*. 27:447-452.
17. Kempermann G, Song H, Gage FH (2015): Neurogenesis in the Adult Hippocampus. *Cold Spring Harb Perspect Biol*. 7:a018812.
18. van Strien NM, Cappaert NL, Witter MP (2009): The anatomy of memory: an interactive overview of the parahippocampal-hippocampal network. *Nat Rev Neurosci*. 10:272-282.
19. Jessberger S, Clark RE, Broadbent NJ, Clemenson GD, Jr., Consiglio A, Lie DC, et al. (2009): Dentate gyrus-specific knockdown of adult neurogenesis impairs spatial and object recognition memory in adult rats. *Learn Mem*. 16:147-154.
20. Lima SMA, Gomes-Leal W (2019): Neurogenesis in the hippocampus of adult humans: controversy "fixed" at last. *Neural Regen Res*. 14:1917-1918.
21. Yoon K, Gaiano N (2005): Notch signaling in the mammalian central nervous system: insights from mouse mutants. *Nat Neurosci*. 8:709-715.
22. Stump G, Durrer A, Klein AL, Lutolf S, Suter U, Taylor V (2002): Notch1 and its ligands Delta-like and Jagged are expressed and active in distinct cell populations in the postnatal mouse brain. *Mech Dev*. 114:153-159.
23. Ables JL, Breunig JJ, Eisch AJ, Rakic P (2011): Not(ch) just development: Notch signalling in the adult brain. *Nat Rev Neurosci*. 12:269-283.

24. Ehm O, Goritz C, Covic M, Schaffner I, Schwarz TJ, Karaca E, et al. (2010): RBPJkappa-dependent signaling is essential for long-term maintenance of neural stem cells in the adult hippocampus. *J Neurosci*. 30:13794-13807.
25. Kopan R, Ilagan MX (2009): The canonical Notch signaling pathway: unfolding the activation mechanism. *Cell*. 137:216-233.
26. Schmidt MH, Bicker F, Nikolic I, Meister J, Babuke T, Picuric S, et al. (2009): Epidermal growth factor-like domain 7 (EGFL7) modulates Notch signalling and affects neural stem cell renewal. *Nat Cell Biol*. 11:873-880. doi: 810.1038/ncb1896. Epub 2009 Jun 1037.
27. Bicker F, Vasic V, Horta G, Ortega F, Nolte H, Kavyanifar A, et al. (2017): Neurovascular EGFL7 regulates adult neurogenesis in the subventricular zone and thereby affects olfactory perception. *Nat Commun*. 8:15922.
28. Bicker F, Schmidt MHH (2010): EGFL7: a new player in homeostasis of the nervous system. *Cell Cycle*. 9:1263-1269.
29. Larochelle C, Uphaus T, Broux B, Gowing E, Paterka M, Michel L, et al. (2018): EGFL7 reduces CNS inflammation in mouse. *Nat Commun*. 9:819.
30. Nikolic I, Stankovic ND, Bicker F, Meister J, Braun H, Awwad K, et al. (2013): EGFL7 ligates alphavbeta3 integrin to enhance vessel formation. *Blood*. 121:3041-3050.
31. Jolivel V, Bicker F, Biname F, Ploen R, Keller S, Gollan R, et al. (2015): Perivascular microglia promote blood vessel disintegration in the ischemic penumbra. *Acta Neuropathol*. 129:279-295. doi: 210.1007/s00401-00014-01372-00401. Epub 02014 Dec 00413.
32. Schmidt M, Paes K, De Maziere A, Smyczek T, Yang S, Gray A, et al. (2007): EGFL7 regulates the collective migration of endothelial cells by restricting their spatial distribution. *Development*. 134:2913-2923.
33. Kim EJ, Ables JL, Dickel LK, Eisch AJ, Johnson JE (2011): Ascl1 (Mash1) defines cells with long-term neurogenic potential in subgranular and subventricular zones in adult mouse brain. *PLoS One*. 6:e18472.
34. Zhang J, Giesert F, Kloos K, Vogt Weisenhorn DM, Aigner L, Wurst W, et al. (2010): A powerful transgenic tool for fate mapping and functional analysis of newly generated neurons. *BMC Neurosci*. 11:158.
35. Lakso M, Pichel JG, Gorman JR, Sauer B, Okamoto Y, Lee E, et al. (1996): Efficient in vivo manipulation of mouse genomic sequences at the zygote stage. *Proc Natl Acad Sci U S A*. 93:5860-5865.
36. Codega P, Silva-Vargas V, Paul A, Maldonado-Soto AR, Deleo AM, Pastrana E, et al. (2014): Prospective identification and purification of quiescent adult neural stem cells from their in vivo niche. *Neuron*. 82:545-559.
37. Wingett SW, Andrews S (2018): FastQ Screen: A tool for multi-genome mapping and quality control. *F1000Res*. 7:1338.
38. Waterston RH, Lindblad-Toh K, Birney E, Rogers J, Abril JF, Agarwal P, et al. (2002): Initial sequencing and comparative analysis of the mouse genome. *Nature*. 420:520-562.
39. Subramanian A, Tamayo P, Mootha VK, Mukherjee S, Ebert BL, Gillette MA, et al. (2005): Gene set enrichment analysis: a knowledge-based approach for interpreting genome-wide expression profiles. *Proc Natl Acad Sci U S A*. 102:15545-15550.
40. Morris R (1984): Developments of a water-maze procedure for studying spatial learning in the rat. *J Neurosci Methods*. 11:47-60.
41. Albuquerque B, Haussler A, Vannoni E, Wolfer DP, Tegeder I (2013): Learning and memory with neuropathic pain: impact of old age and progranulin deficiency. *Frontiers in behavioral neuroscience*. 7:174.
42. Hardt S, Heidler J, Albuquerque B, Valek L, Altmann C, Wilken-Schmitz A, et al. (2017): Loss of synaptic zinc transport in progranulin deficient mice may contribute to progranulin-associated psychopathology and chronic pain. *Biochimica et biophysica acta*. 1863:2727-2745.
43. Hardt S, Fischer C, Vogel A, Wilken-Schmitz A, Tegeder I (2019): Distal infraorbital nerve injury (DIONI): a model for persistent facial pain in mice. *Pain*.

44. Krackow S, Vannoni E, Codita A, Mohammed AH, Cirulli F, Branchi I, et al. (2010): Consistent behavioral phenotype differences between inbred mouse strains in the IntelliCage. *Genes Brain Behav*. 9:722-731.
45. Silverman JL, Gastrell PT, Karras MN, Solomon M, Crawley JN (2015): Cognitive abilities on transitive inference using a novel touchscreen technology for mice. *Cereb Cortex*. 25:1133-1142.
46. Izquierdo A, Wiedholz LM, Millstein RA, Yang RJ, Bussey TJ, Saksida LM, et al. (2006): Genetic and dopaminergic modulation of reversal learning in a touchscreen-based operant procedure for mice. *Behav Brain Res*. 171:181-188.
47. Horner AE, Heath CJ, Hvoslef-Eide M, Kent BA, Kim CH, Nilsson SR, et al. (2013): The touchscreen operant platform for testing learning and memory in rats and mice. *Nat Protoc*. 8:1961-1984. doi: 1910.1038/nprot.2013.1122. Epub 2013 Sep 1919.
48. Brigman JL, Feyder M, Saksida LM, Bussey TJ, Mishina M, Holmes A (2008): Impaired discrimination learning in mice lacking the NMDA receptor NR2A subunit. *Learn Mem*. 15:50-54.
49. Brigman JL, Daut RA, Saksida L, Bussey TJ, Nakazawa K, Holmes A (2015): Impaired discrimination learning in interneuronal NMDAR-GluN2B mutant mice. *Neuroreport*. 26:489-494.
50. Gould RW, Dencker D, Grannan M, Bubser M, Zhan X, Wess J, et al. (2015): Role for the M1 Muscarinic Acetylcholine Receptor in Top-Down Cognitive Processing Using a Touchscreen Visual Discrimination Task in Mice. *ACS Chem Neurosci*. 6:1683-1695.
51. Zeleznikow-Johnston AM, Renoir T, Churilov L, Li S, Burrows EL, Hannan AJ (2018): Touchscreen testing reveals clinically relevant cognitive abnormalities in a mouse model of schizophrenia lacking metabotropic glutamate receptor 5. *Sci Rep*. 8:16412.
52. Lacko LA, Massimiani M, Sones JL, Hurtado R, Salvi S, Ferrazzani S, et al. (2014): Novel expression of EGFL7 in placental trophoblast and endothelial cells and its implication in preeclampsia. *Mech Dev*. 133:163-176.
53. van Praag H, Kempermann G, Gage FH (1999): Running increases cell proliferation and neurogenesis in the adult mouse dentate gyrus. *Nat Neurosci*. 2:266-270.
54. Mauceri D, Buchthal B, Hemstedt TJ, Weiss U, Klein CD, Bading H (2020): Nasally delivered VEGFD mimetics mitigate stroke-induced dendrite loss and brain damage. *Proc Natl Acad Sci U S A*. 117:8616-8623.
55. Bourne J, Harris KM (2007): Do thin spines learn to be mushroom spines that remember? *Curr Opin Neurobiol*. 17:381-386.
56. Talpos JC, Fletcher AC, Circelli C, Tricklebank MD, Dix SL (2012): The pharmacological sensitivity of a touchscreen-based visual discrimination task in the rat using simple and perceptually challenging stimuli. *Psychopharmacology (Berl)*. 221:437-449.
57. Romberg C, Bartko S, Wess J, Saksida LM, Bussey TJ (2018): Impaired object-location learning and recognition memory but enhanced sustained attention in M2 muscarinic receptor-deficient mice. *Psychopharmacology (Berl)*. 235:3495-3508.
58. Fischer C, Endle H, Schumann L, Wilken-Schmitz A, Kaiser J, Gerber S, et al. (2020): Prevention of age-associated neuronal hyperexcitability with improved learning and attention upon knockout or antagonism of LPAR2. *Cell Mol Life Sci*.
59. Tran BN, Valek L, Wilken-Schmitz A, Fuhrmann DC, Namgaladze, Wittig I, et al. (2021): Reduced exploratory behavior in neuronal nucleoredoxin knockout mice. *Redox Biol*. (accepted).
60. Casse F, Richetin K, Toni N (2018): Astrocytes' Contribution to Adult Neurogenesis in Physiology and Alzheimer's Disease. *Front Cell Neurosci*. 12:432.
61. Licht T, Keshet E (2015): The vascular niche in adult neurogenesis. *Mech Dev*. 138 Pt 1:56-62.
62. Vicidomini C, Guo N, Sahay A (2020): Communication, Cross Talk, and Signal Integration in the Adult Hippocampal Neurogenic Niche. *Neuron*. 105:220-235.
63. Merkle FT, Tramontin AD, Garcia-Verdugo JM, Alvarez-Buylla A (2004): Radial glia give rise to adult neural stem cells in the subventricular zone. *Proc Natl Acad Sci U S A*. 101:17528-17532.
64. Filippov V, Kronenberg G, Pivneva T, Reuter K, Steiner B, Wang LP, et al. (2003): Subpopulation of nestin-expressing progenitor cells in the adult murine hippocampus shows electrophysiological and morphological characteristics of astrocytes. *Mol Cell Neurosci*. 23:373-382.

65. Moss J, Gebara E, Bushong EA, Sanchez-Pascual I, O'Laoi R, El M'Ghari I, et al. (2016): Fine processes of Nestin-GFP-positive radial glia-like stem cells in the adult dentate gyrus ensheathe local synapses and vasculature. *Proc Natl Acad Sci U S A*. 113:E2536-2545.
66. Li Y, Guo W (2020): Neural Stem Cell Niche and Adult Neurogenesis. *Neuroscientist*.1073858420939034.
67. Lois C, Garcia-Verdugo JM, Alvarez-Buylla A (1996): Chain migration of neuronal precursors. *Science*. 271:978-981.
68. Peretto P, Merighi A, Fasolo A, Bonfanti L (1997): Glial tubes in the rostral migratory stream of the adult rat. *Brain Res Bull*. 42:9-21.
69. Lledo PM, Merkle FT, Alvarez-Buylla A (2008): Origin and function of olfactory bulb interneuron diversity. *Trends Neurosci*. 31:392-400.
70. Toda T, Parylak SL, Linker SB, Gage FH (2019): The role of adult hippocampal neurogenesis in brain health and disease. *Mol Psychiatry*. 24:67-87.
71. Cameron HA, McKay RD (2001): Adult neurogenesis produces a large pool of new granule cells in the dentate gyrus. *J Comp Neurol*. 435:406-417.
72. Moreno-Jimenez EP, Flor-Garcia M, Terreros-Roncal J, Rabano A, Cafini F, Pallas-Bazarra N, et al. (2019): Adult hippocampal neurogenesis is abundant in neurologically healthy subjects and drops sharply in patients with Alzheimer's disease. *Nat Med*. 25:554-560.
73. Bergmann O, Liebl J, Bernard S, Alkass K, Yeung MS, Steier P, et al. (2012): The age of olfactory bulb neurons in humans. *Neuron*. 74:634-639.
74. Lazarov O, Hollands C (2016): Hippocampal neurogenesis: Learning to remember. *Prog Neurobiol*. 138-140:1-18.
75. Breunig JJ, Silbereis J, Vaccarino FM, Sestan N, Rakic P (2007): Notch regulates cell fate and dendrite morphology of newborn neurons in the postnatal dentate gyrus. *Proc Natl Acad Sci U S A*. 104:20558-20563.
76. Ables JL, Decarolis NA, Johnson MA, Rivera PD, Gao Z, Cooper DC, et al. (2010): Notch1 is required for maintenance of the reservoir of adult hippocampal stem cells. *J Neurosci*. 30:10484-10492.
77. Imayoshi I, Sakamoto M, Yamaguchi M, Mori K, Kageyama R (2010): Essential roles of Notch signaling in maintenance of neural stem cells in developing and adult brains. *J Neurosci*. 30:3489-3498.
78. Han J, Calvo CF, Kang TH, Baker KL, Park JH, Parras C, et al. (2015): Vascular endothelial growth factor receptor 3 controls neural stem cell activation in mice and humans. *Cell Rep*. 10:1158-1172.
79. Xie Q, Cheng J, Pan G, Wu S, Hu Q, Jiang H, et al. (2019): Treadmill exercise ameliorates focal cerebral ischemia/reperfusion-induced neurological deficit by promoting dendritic modification and synaptic plasticity via upregulating caveolin-1/VEGF signaling pathways. *Exp Neurol*. 313:60-78.
80. Kasai H, Matsuzaki M, Noguchi J, Yasumatsu N, Nakahara H (2003): Structure-stability-function relationships of dendritic spines. *Trends Neurosci*. 26:360-368.
81. Tada T, Sheng M (2006): Molecular mechanisms of dendritic spine morphogenesis. *Curr Opin Neurobiol*. 16:95-101.
82. Wosiski-Kuhn M, Stranahan AM (2012): Transient increases in dendritic spine density contribute to dentate gyrus long-term potentiation. *Synapse*. 66:661-664.
83. Aimone JB, Deng W, Gage FH (2011): Resolving new memories: a critical look at the dentate gyrus, adult neurogenesis, and pattern separation. *Neuron*. 70:589-596.
84. Yassa MA, Stark CE (2011): Pattern separation in the hippocampus. *Trends Neurosci*. 34:515-525.
85. Kempermann G (2019): Environmental enrichment, new neurons and the neurobiology of individuality. *Nat Rev Neurosci*. 20:235-245.
86. Lepousez G, Nissant A, Lledo PM (2015): Adult neurogenesis and the future of the rejuvenating brain circuits. *Neuron*. 86:387-401. doi: 310.1016/j.neuron.2015.1001.1002.

87. Libert S, Cohen D, Guarente L (2008): Neurogenesis directed by Sirt1. *Nat Cell Biol*. 10:373-374.
88. Suwabe K, Hyodo K, Byun K, Ochi G, Yassa MA, Soya H (2017): Acute moderate exercise improves mnemonic discrimination in young adults. *Hippocampus*. 27:229-234.
89. Suwabe K, Byun K, Hyodo K, Reagh ZM, Roberts JM, Matsushita A, et al. (2018): Rapid stimulation of human dentate gyrus function with acute mild exercise. *Proc Natl Acad Sci U S A*. 115:10487-10492.
90. Mirochnic S, Wolf S, Staufenbiel M, Kempermann G (2009): Age effects on the regulation of adult hippocampal neurogenesis by physical activity and environmental enrichment in the APP23 mouse model of Alzheimer disease. *Hippocampus*. 19:1008-1018.
91. Jain S, Yoon SY, Zhu L, Brodbeck J, Dai J, Walker D, et al. (2012): Arf4 determines dentate gyrus-mediated pattern separation by regulating dendritic spine development. *PLoS One*. 7:e46340.
92. Han W, Song X, He R, Li T, Cheng L, Xie L, et al. (2017): VEGF regulates hippocampal neurogenesis and reverses cognitive deficits in immature rats after status epilepticus through the VEGF R2 signaling pathway. *Epilepsy Behav*. 68:159-167.
93. Pombero A, Garcia-Lopez R, Estirado A, Martinez S (2018): Vascular pattern of the dentate gyrus is regulated by neural progenitors. *Brain structure & function*. 223:1971-1987.
94. Lin R, Cai J, Kenyon L, Iozzo R, Rosenwasser R, Iacovitti L (2019): Systemic Factors Trigger Vasculature Cells to Drive Notch Signaling and Neurogenesis in Neural Stem Cells in the Adult Brain. *Stem Cells*. 37:395-406.
95. Kalm M, Karlsson N, Nilsson MK, Blomgren K (2013): Loss of hippocampal neurogenesis, increased novelty-induced activity, decreased home cage activity, and impaired reversal learning one year after irradiation of the young mouse brain. *Exp Neurol*.
96. Garthe A, Roeder I, Kempermann G (2016): Mice in an enriched environment learn more flexibly because of adult hippocampal neurogenesis. *Hippocampus*. 26:261-271.
97. Vogel A, Wilken-Schmitz A, Hummel R, Lang M, Trautmann S, Gurke R, et al. (2020): Low brain endocannabinoids associated with persistent non-goal directed nighttime hyperactivity after traumatic brain injury in mice. *Sci Rep*. accepted.
98. McGann JP (2017): Poor human olfaction is a 19th-century myth. *Science*. 356.

## Figure legends

### Figure 1. Localization of EGFL7 in the human and mouse dentate gyrus

(**a**) Immunofluorescence staining revealed EGFL7 expression in granule cells and larger blood vessels of the human dentate gyrus as well as larger neurons of the hilus. Scale bars represent 50 µm or 10 µm (magnification). (**b**) Furthermore, EGFL7 was expressed in the dentate gyrus of mice as detected by fluorescence *in situ* hybridization (FISH). Scale bars represent 50 µm or 10 µm (magnification). (**c**) Cells of murine hippocampi were isolated by fluorescence-activated cell sorting using a combination of the following markers: $GFAP^+/CD133^+/EGFR^-$ for quiescent neural stem cells (qNSCs), $GFAP^+/CD133^+/EGFR^+$ for active NSCs (aNSC), $GLAST^-/CD133^-/EGFR^+$ for neural progenitor cells (NPCs), $CD24^+$ for neuroblasts (NBs), $Thy\text{-}GFP1^+$ for neurons and $CD31^+$ for endothelial cells (ECs). Expression of *Egfl7* was measured by quantitative reverse transcriptase-polymerase chain reaction using two housekeeping genes and data was plotted as normalized to unsorted hippocampus tissue (HC). Data are presented as mean values with 95% confidence interval (CI). (**d**) EGFL7-specific FISH probes in combination with cell type-specific markers verified EGFL7-expression in aNSCs/NPCs (Stmn1; arrowheads) and neurons (NeuN; arrowheads). Scale bars represent 10 µm.

### Figure 2. EGFL7 governs proliferation of neural stem cells in the hippocampus

(**a**) Representative images of neural stem and progenitor cells isolated from mouse hippocampus (HC) and cultured as spheres. Scale bars represent 25 µm. (**b**) Size of *EGFL7*-/- neurospheres was increased (58.95 ± 11.24 µm (n = 5) versus 43.85 ± 2.25 µm in wild-type control (WT); n = 4; $p = 0.0317$). (**c**) Fluorescence-activated cell sorting revealed an increase in activated neural stem cells (aNSCs) in *EGFL7*-/- mice (5.56 ± 1.65% versus 2.20 ± 0.53% in WT, n = 3; $p = 0.0499$) but about equal amounts of quiescent qNSCs. (**d**) Flow cytometry-based cell cycle analysis of *EGFL7*-/- and WT neurospheres yielded an increased amount of cells in the G2/M phase in *EGFL7*-/- mice (33.65 ± 6.10% versus 25.10 ± 2.03%; n = 3; $p = 0.0286$). (**e**) The paradigm used for cell cycle analysis *in vivo*. (**f**) Representative images of the dentate gyrus 1 h post administration of CldU. Quantification

of cells yielded an increased amount of cells in S phase in *EGFL7*-/- mice (11.00 ± 2.71 versus 5.25 ± 1.71 cells per section in WT; n = 4; $p = 0.0571$). (**g**) Representative images of the dentate gyrus 24 h post administration of IdU and double-stained for Ki67/IdU. Quantification revealed sustained proliferation in *EGFL7*-/- mice (17.25 ± 2.06 versus 10.00 ± 2.45 cells per section in WT; n = 4; $p = 0.0286$). Scale bars represent 90 µm. Statistical analysis was performed by Mann–Whitney *U*-test. Data are represented as mean ± SEM; $^{*}p < 0.05$.

**Figure 3. Loss-of-EGFL7 upregulates neurogenesis in the hippocampus**

(**a**) Markers used in immunofluorescence analyses (IF) to label specific cell types of neural stem cell (NSC) differentiation in the dentate gyrus (DG): GFAP/Nestin for NSCs (type 1), Stmn1 for activated aNSCs and neural precursor cells (NPCs, type 1, type 2), Mash1 for aNSCs/type 2a cells, DCX for type 2b/type 3 and immature neurons, NeuN for mature neurons and granule cells. (**b**) Experimental paradigms of applied neurogenesis assays. (**c**) Quantitative analyses revealed that NSCs ($GFAP^+/Nestin^+/BrdU^+$) remained unchanged in *EGFL7*-/- mice (10.50 ± 3.51 versus 11.00 ± 1.41 cells per section in wild-type controls (WT); n = 4; $p > 0.9999$). (**d**) The number of type 2a ($BrdU^+/Mash1^+$) cells was increased (11.25 ± 1.71 versus 3.00 ± 0.82 in WT; n = 4; $p = 0.0286$). (**e**) Type 2b/type 3 ($BrdU^+/DCX^+$) cells were decreased (7.00 ± 2.16 versus 14.75 ± 5.56 cells per section in WT; n = 4; $p = 0.0286$). (**f**) The amount of aNSCs/NPCs ($BrdU^+/Stmn1^+$) was strongly increased in the DG of *EGFL7*-/- animals (18.25 ± 4.99 versus 5.25 ± 3.59 cells per section in WT; n = 4; $p = 0.0286$). (**g**) Last, more newborn neurons ($BrdU^+/NeuN^+$) were formed in the DG of *EGFL7*-/- mice (21.50 ± 4.12 versus 5.75 ± 4.35 cells per section in WT; n = 4; $p = 0.0286$). Statistical analysis was performed by Mann-Whitney *U*-test. Data are represented as mean ± SEM; * $p < 0.05$. Scale bars represent 60 µm.

**Figure 4. EGFL7 deletion in neural progenitors phenocopies the global EGFL7 knock-out**

(**a**) Description of the *EGFL7 fl/fl;Ascl1-CreERT2* mouse model allowing for a tamoxifen-inducible, type 2a cell-specific knock-out of EGFL7. (**b**) Experimental paradigms of applied neurogenesis assays. (**c**) The amount of aNSCs/NPCs ($BrdU^+/Mash1^+$) were found to be increased (5.25 ± 2.63 versus 1.00 ± 1.15 cells per section in *EGFL7 fl/fl*; n = 4; $p = 0.0286$). (**d**) The number of type 2b/type 3 cells ($BrdU^+/DCX^+$) was decreased in *EGFL7 del;Ascl1-CreERT2* mice (8.50 ± 5.51 versus 18.75 ± 2.22 in *EGFL7 fl/fl*; n = 4; $p = 0.0286$), (**e**) while quantification of $BrdU^+/Stmn1^+$ activated neural stem and precursor cells (aNSCs/NPCs) revealed a significant upregulation in EGFL7 del*;Ascl1-CreERT2* mice (20.25 ± 3.10 versus 8.00 ± 4.24 cells per section in *EGFL7 fl/fl* control; n = 4; $p = 0.0286$). (**f**) Futhermore, the amount of adult-born neurons ($BrdU^+/NeuN^+$) was increased (18.25 ± 6.80 versus 5.50 ± 2.65 cells per section in *EGFL7 fl/fl*; n = 4; $p = 0.0286$). Statistical analysis was performed by Mann-Whitney *U*-test. Data are represented as mean ± SEM; $*p < 0.05$; Scale bars represent 60 µm.

**Figure 5. Upregulation of VEGF-D upon EGFL7 knock-out**

(**a**) Volcano and (**b**) MA plots of RNA-sequencing-based transcriptomics in neural stem and precursor cells confirmed EGFL7 knock-out and identified an upregulation of the cytokine VEGF-D (n = 4 for each genotype; two datasets). Volcano plots illustrate the Log2 difference (i.e., fold change) versus -logP of the t-test. MA plots display the LOG2 difference versus the mean expression level (LOG2 RPKM). The VENN diagrams show the agreement of experiment 1 and 2 and the combined analysis of regulated candidates, based on P value and fold change. (**c**) Upregulation of VEGF-D upon EGFL7 knock-out was confirmed by quantitative reverse transcriptase-polymerase chain reaction (6.56 ± 2.85 versus 1.47 ± 0.61 in wild-type control (WT); n = 3; $p = 0.039$). (**d**) Expression of VEGF-D in the dentate gyrus of the hippocampus was visualized by immunofluorescent staining using a VEGF-D-specific antibody. Statistical analysis was performed by Student's t-test. Data are represented as mean ± SEM; $*p < 0.05$. Scale bars represent 90 µm or 45 µm (magnifications).

**Figure 6. VEGF-D stimulates neurogenesis *in vivo***

(**a**) Recombinant, purified VEGF-D was infused in the dentate gyrus of mice using osmotic pumps. (**b**) Experimental paradigm to study neurogenesis in this setup. (**c**) CldU staining in the dentate gyrus revealed a significant increase in proliferation upon infusion of recombinant, purified VEGF-D (51.00 ± 19.43 versus 16.20 ± 3.03 cells per section in wild-type control (WT); n = 5, $p$ = 0.0079). (**d**) Mash1$^+$/CldU$^+$ precursors were increased upon VEGF-D infusion (10.40 ± 5.13 versus 5.20 ± 0.84 cells per section in WT; n = 5, $p$ = 0.0238). (**e**) So were Stmn1$^+$/CldU$^+$ neural stem and precursor cells (23.00 ± 7.33 versus 7.00 ± 1.00 in WT; n = 5; $p$ = 0.0079). (**f**) Last, maturation of adult-born neurons was enhanced by VEGF-D (35.2 ± 8.29 versus 19.40 ± 4.72 cells per section in WT; n = 5; $p$ = 0.0159). Statistical analysis was performed by Mann-Whitney *U*-test. Data are represented as mean ± SEM; *$p$ < 0.05; Scale bars represent 90 µm (c) or 60 µm (**d-f**).

**Figure 7. Dendritic spine analysis in the HC and primary hippocampal neurons**

(**a**) Representative pictures of analyzed spines of 10-week-old *EGFL7*-/- and WT mice. (**b**) The analysis of DG spines of 10-week-old mice showed increased number of spines in *EGFL7*-/- mice and (**c**) significantly more thin spines. (**d**) Representative pictures of analyzed spines of 20-week-old *EGFL7*-/- and WT mice. (**e**) After 20 weeks the number of spines is unaffected. (**e)** The numbers of thin, stubby and mushroom spines were also not affected. (**g**) The number of dendrites and their total length was found increased in *EGFL7*-/- primary neuron cultures as detected by Map2 IF staining (**h**). (**i**) Timeline for analysis of neurogenesis in aged mice and quantification of BrdU$^+$/NeuN$^+$ newborn neurons across different ages. Statistical analysis was performed by Mann–Whitney *U*-test. Data are represented as mean ± SD; *$p$ < 0.05; n = 3. Scale bar represents 5 µm.

**Figure 8. EGFL7 deficiency improved spatial learning and memory in MWM and IntelliCage in young adult mice**

(**a**) In the Morris water maze (MWM), the latency to reach the visible platform, the proportion of time spent in the platform quarter and the swimming velocity were similar in both genotypes. (**b**) Body weights were similar throughout experiments. Exemplary cohort is shown as mean ± SD. (**c**) *EGFL7*-/- mice reached the hidden platform faster. Escape latency was reduced considering the full-time course (AUCs) and late trials. (**d**) The proportion of time spent in the platform quarter after its removal was increased. For MWM sample sizes were n = 19 for *EGFL7*-/- mice and n = 33 for wild-type littermate controls (WT). Data were compared by paired (visible platform) and unpaired two-sided Student's t-tests, or 2-way ANOVA for time courses. (**e**) In the IntelliCage, *EGFL7*-/- mice maintained longer avoidance of a previously punished corner (air puff), as revealed by a reduced proportion of nosepoke errors (n = 16 per genotype). (**f**) During preference learning in active module times (11-13:00 and 16-18:00 h each day), *EGFL7*-/- mice showed faster relearning to prefer a specified corner upon switching to the opposite side (reversal learning), indicated by a higher accuracy of nosepokes (n = 16 per genotype). Overall activity is shown in (**Supplementary Fig. 8_2**). (**g,h**) During periods in which the learning modules were inactive (doors remain closed, "default-times"), *EGFL7*-/- mice retained higher preference of rewarding corners and the proportion of "memorizers" was higher, the latter defined as 35% accuracy of corner visits (random = 25%). Time course data are represented as mean ± SEM, summarizing data as mean ± SD. The boxes show the interquartile range, the line is the median, and whiskers are plotted minimum to maximum. Scatters represent individual mice. Time courses were compared by 2-way ANOVA and subsequent posthoc t-tests to assess genotype differences at specific time points without multiplicity adjustment for between group comparisons, AUCs were compared with 2-sided unpaired t-tests; * $p < 0.05$.

**Figure 9. EGFL7 deficiency is associated with youthful activity of old mice**

(**a**) Old *EGFL7fl/fl;EIIa-Cre* mice are hyperactive for their age in comparison with *EGFL7fl/fl* control mice (n = 14-15 per group). They were 71-78 weeks old at the onset of the experiments. Time course data show the 12h light/dark rhythms of goal directed corner visits with licks (LVisits, upper) and of exploratory non-goal-directed visits without licks (SVisits, lower). SVisits were particularly high during adaptation periods, dropped in learning periods (grey shaded areas), normalized in learning with mild stress (CUMS) and re-instated in the post-learning/post-CUMS free period. (**b**) Accuracy time courses (proportion of correct nosepokes) were similar in both groups, but *EGFL7fl/fl;EIIa-Cre* animals were moderately better after the first and second reversal. ANOVA n.s. (**c,d**) Paired analyses of trials and successes during the place preference learning (PPL) periods without and with mild stress (CUMS) show the overactivity of *EGFL7fl/fl;EIIa-Cre* mice, but the number of trials needed to reach the criterion of success (35% correct, i.e., 10 % above random) did not differ between genotypes.

Figure 1

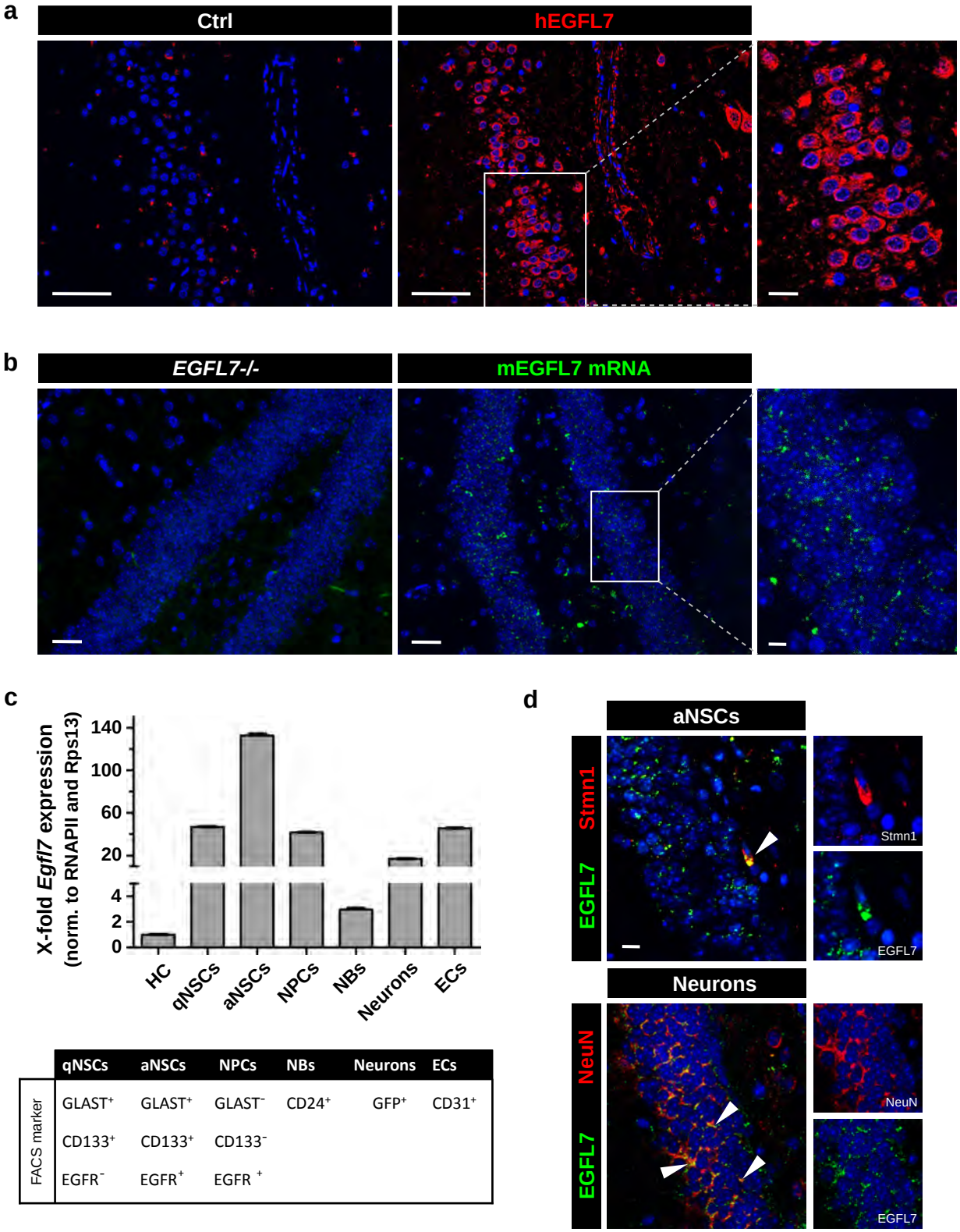


| | qNSCs | aNSCs | NPCs | NBs | Neurons | ECs |
|---|---|---|---|---|---|---|
| FACS marker | GLAST$^+$ | GLAST$^+$ | GLAST$^-$ | CD24$^+$ | GFP$^+$ | CD31$^+$ |
| | CD133$^+$ | CD133$^+$ | CD133$^-$ | | | |
| | EGFR$^-$ | EGFR$^+$ | EGFR $^+$ | | | |

Figure 2



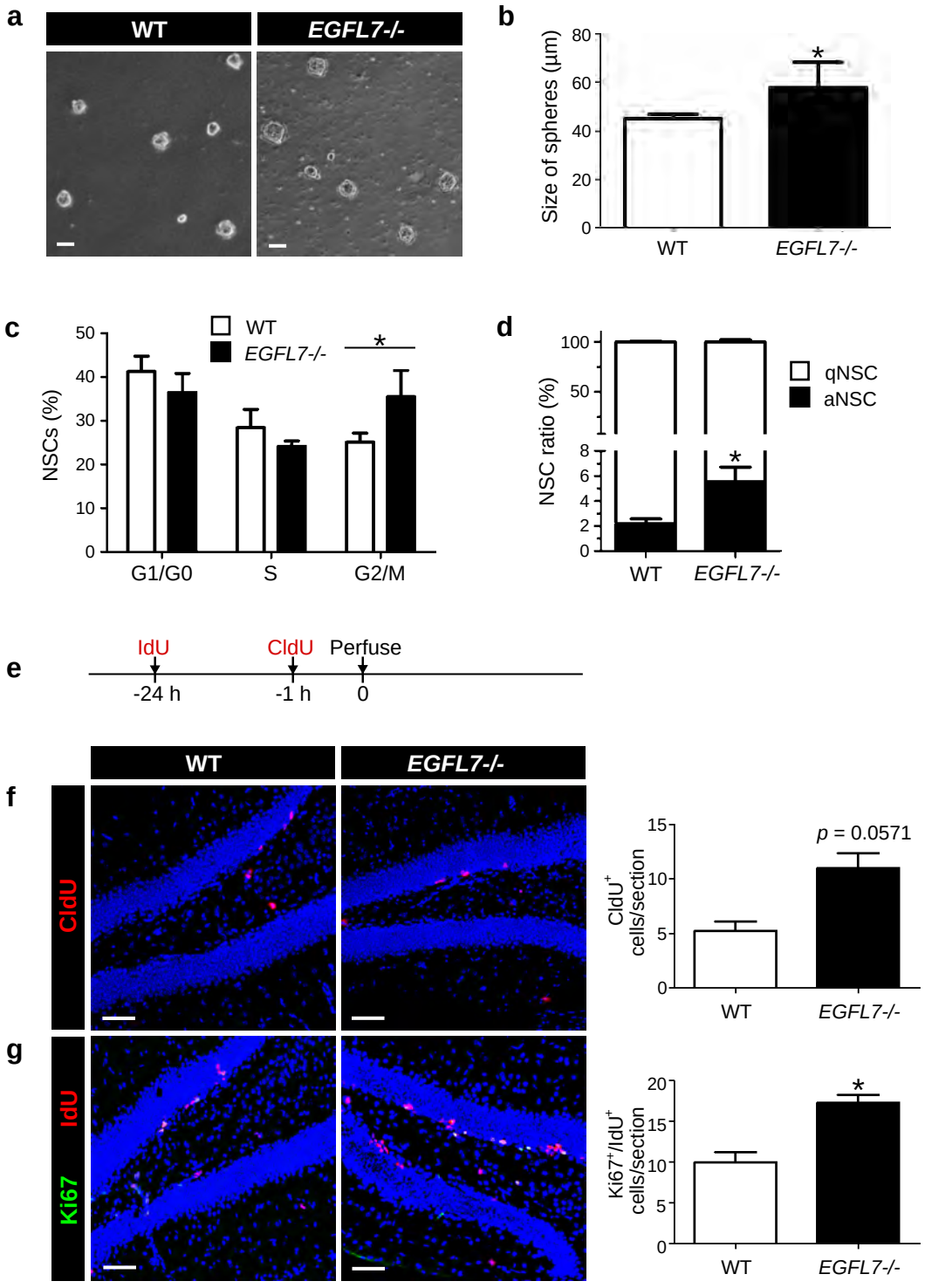

Figure 3



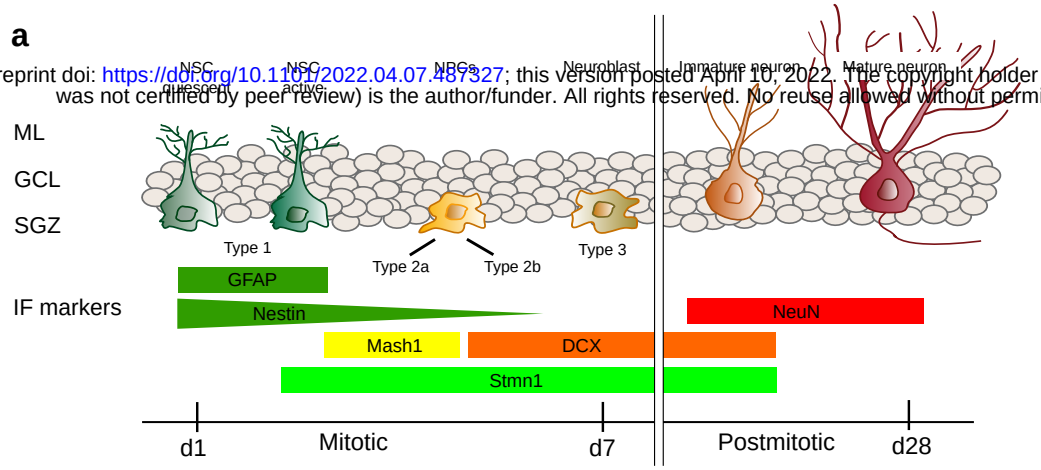


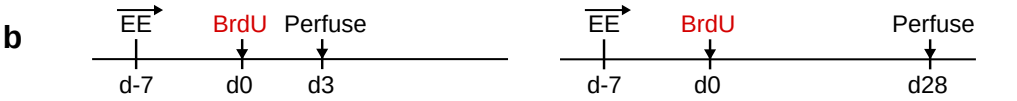


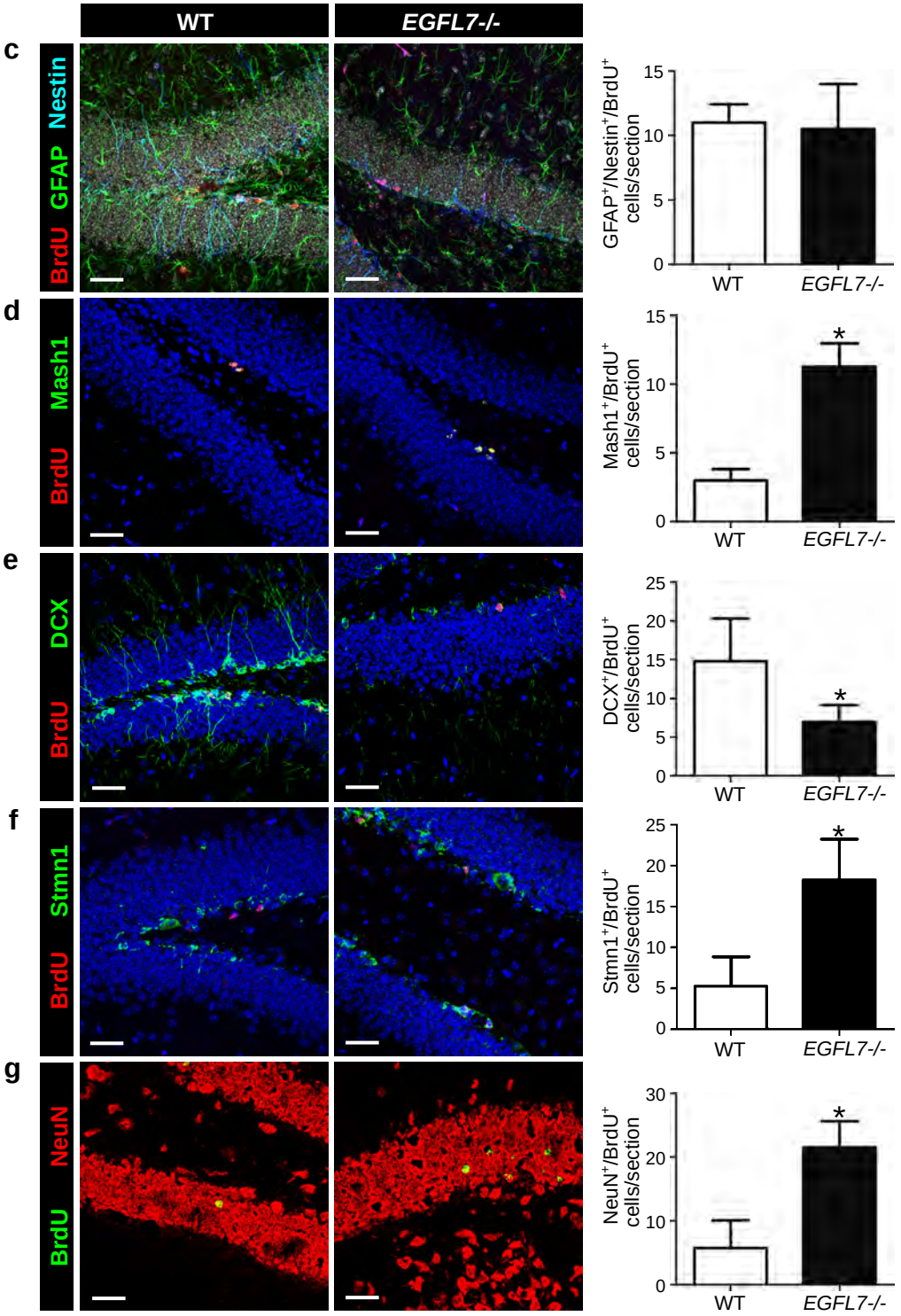

Figure 4



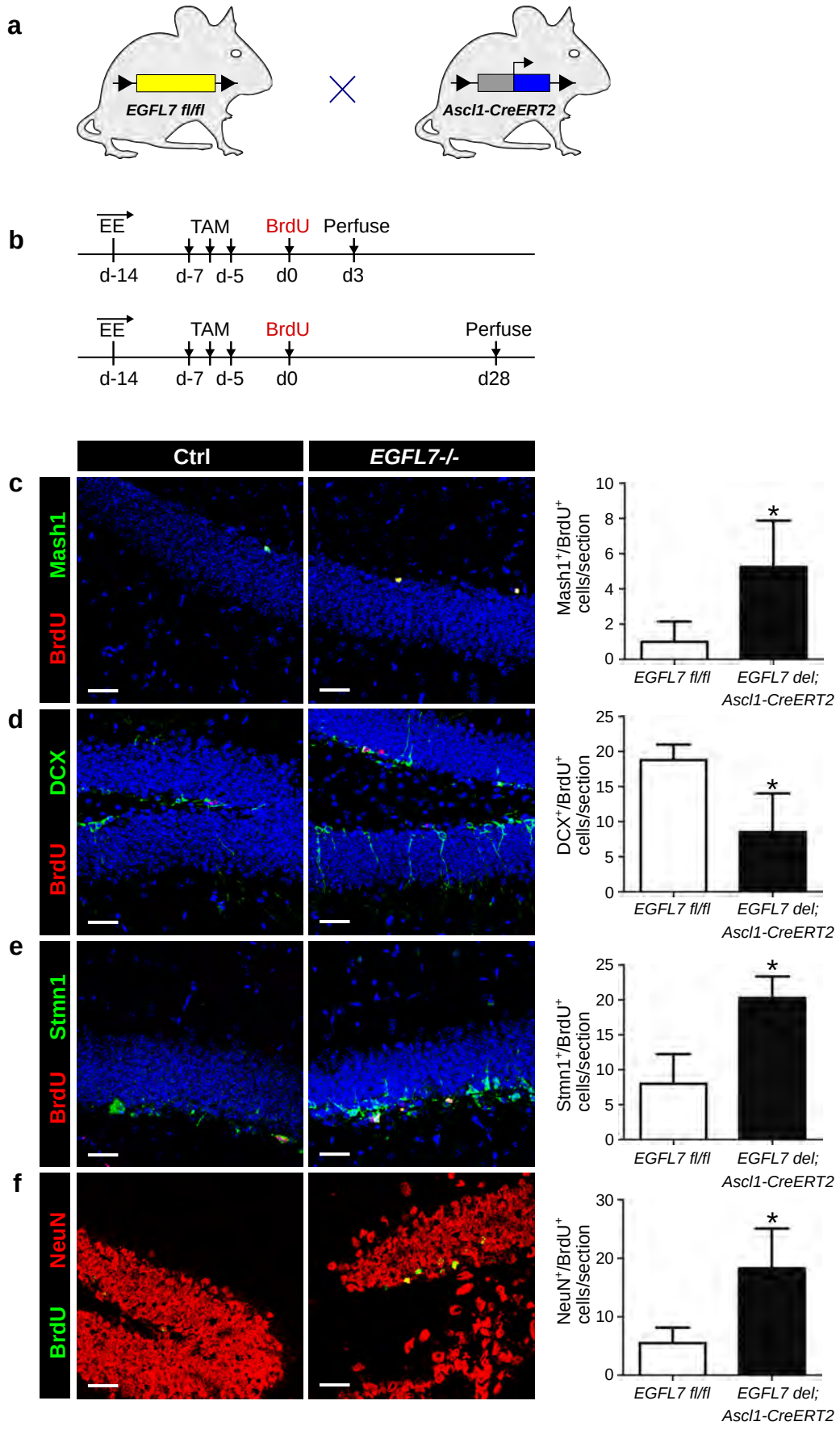

Figure 5

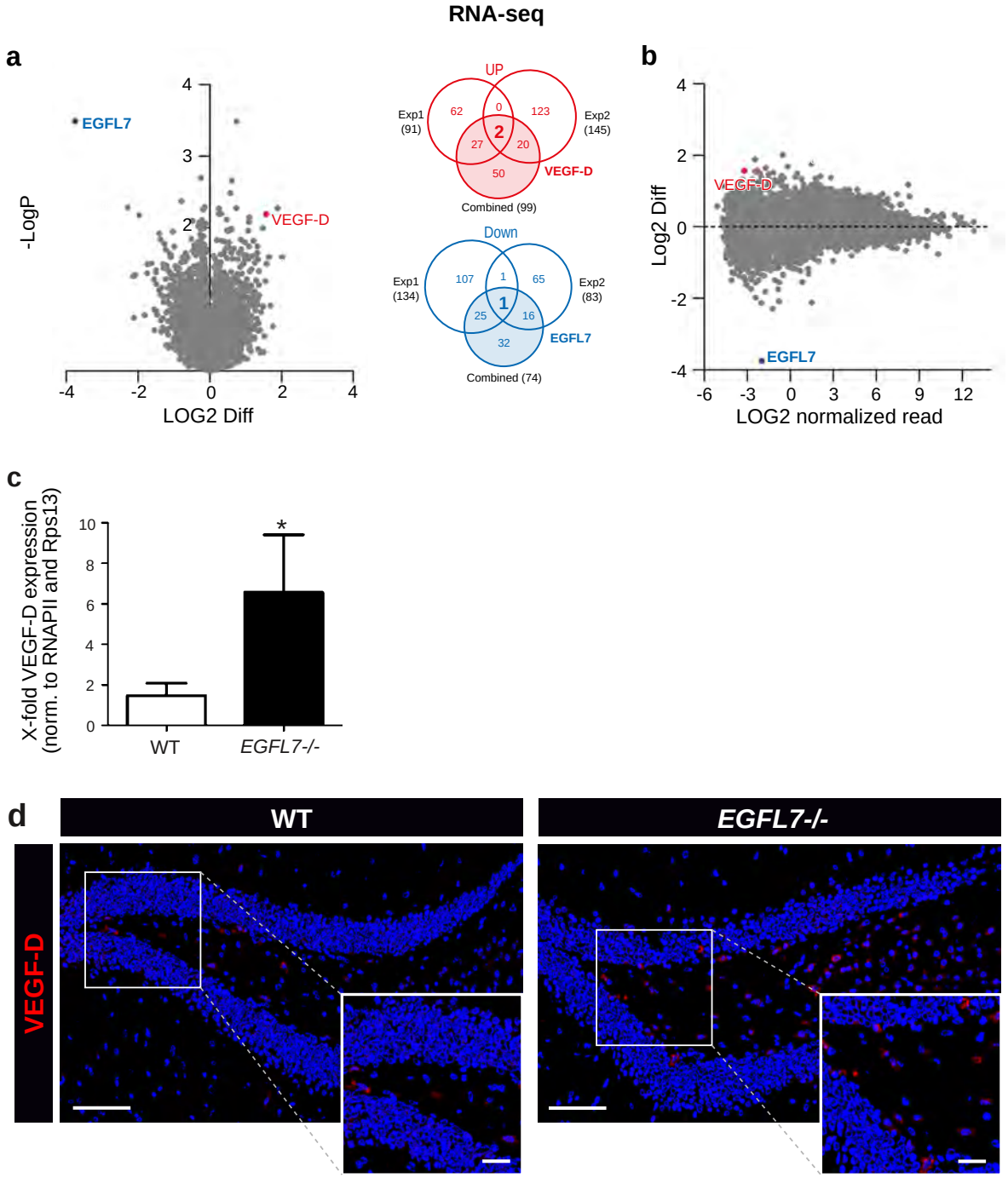

Figure 6

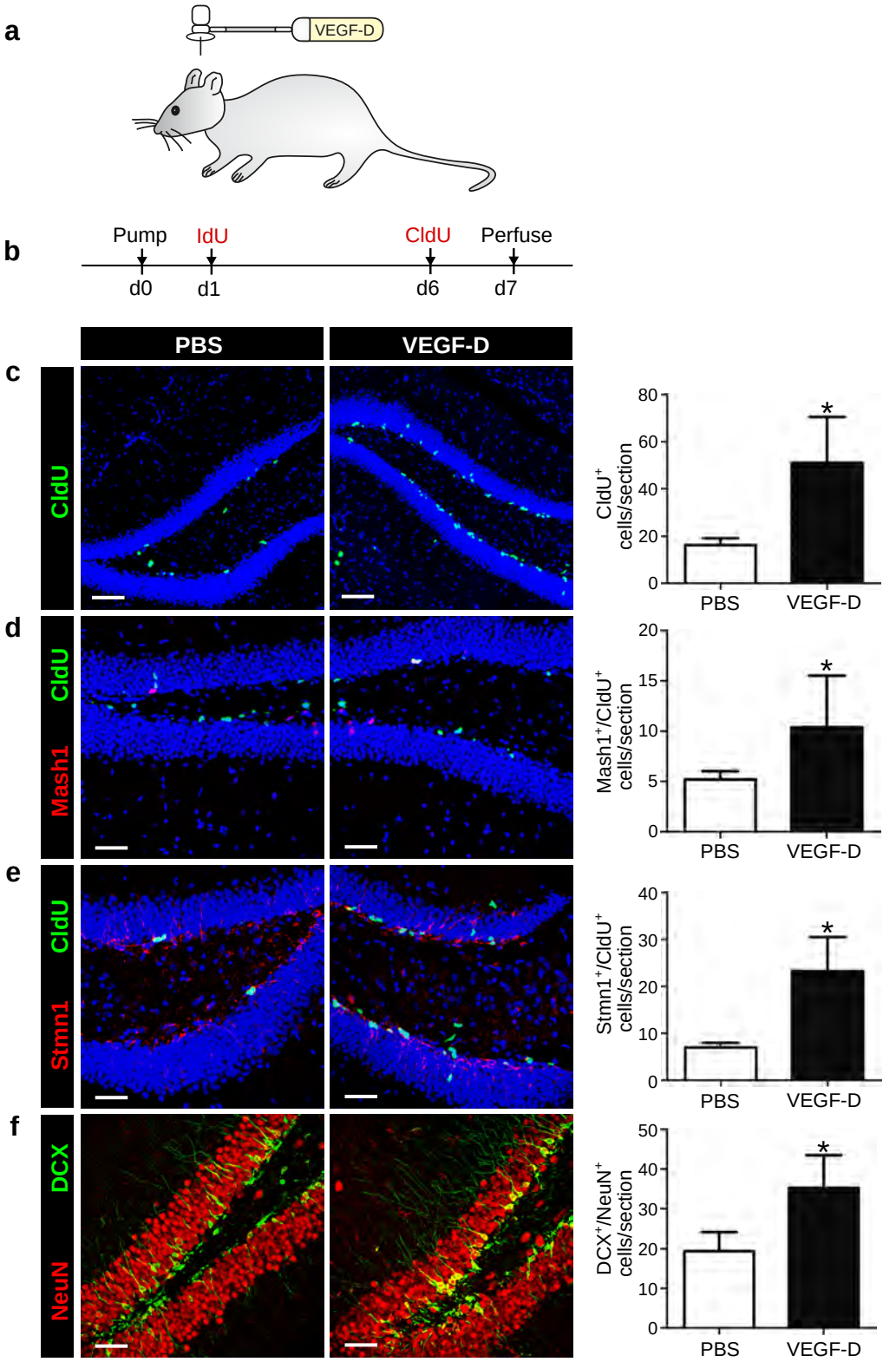

Figure 7



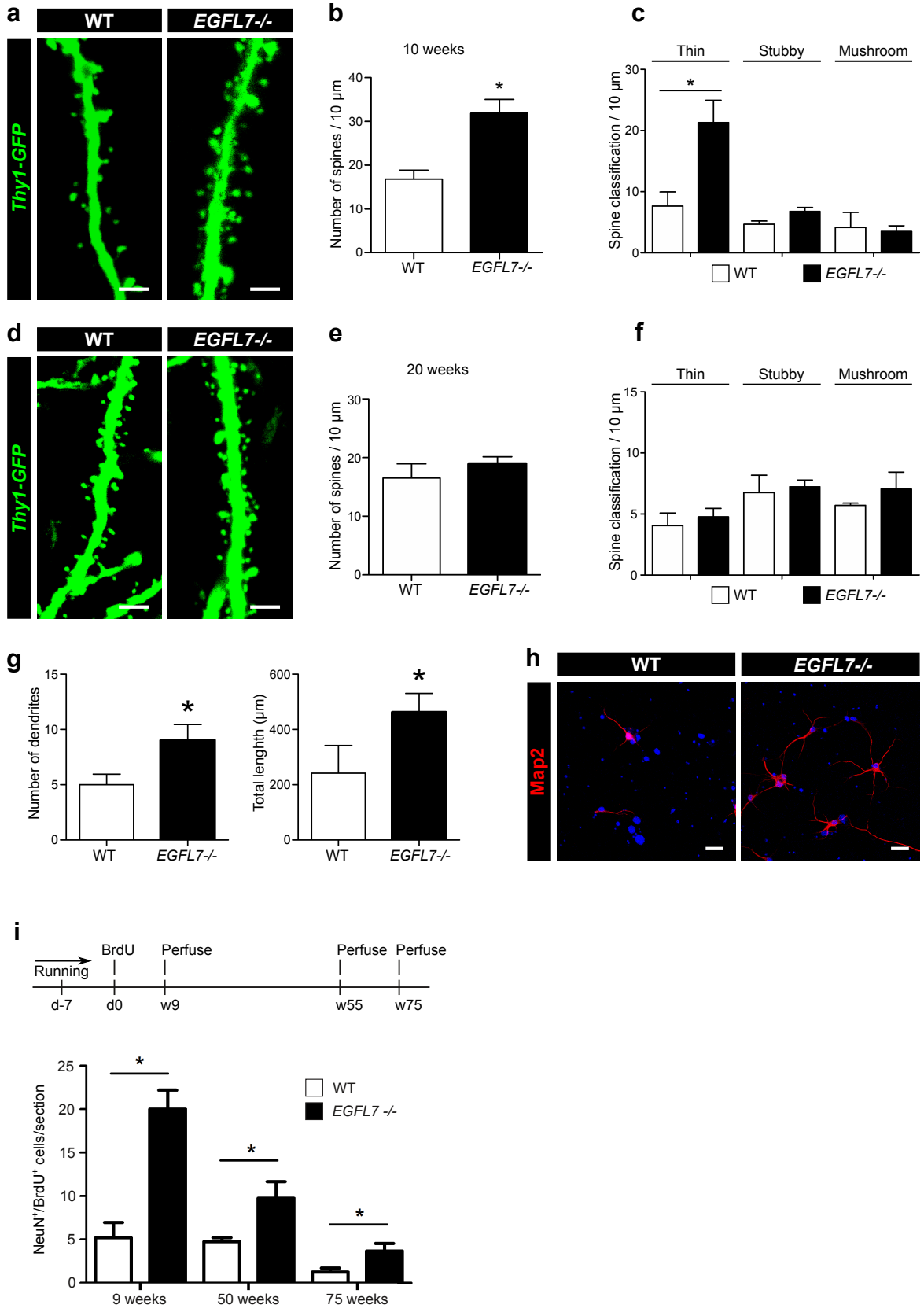

Figure 8



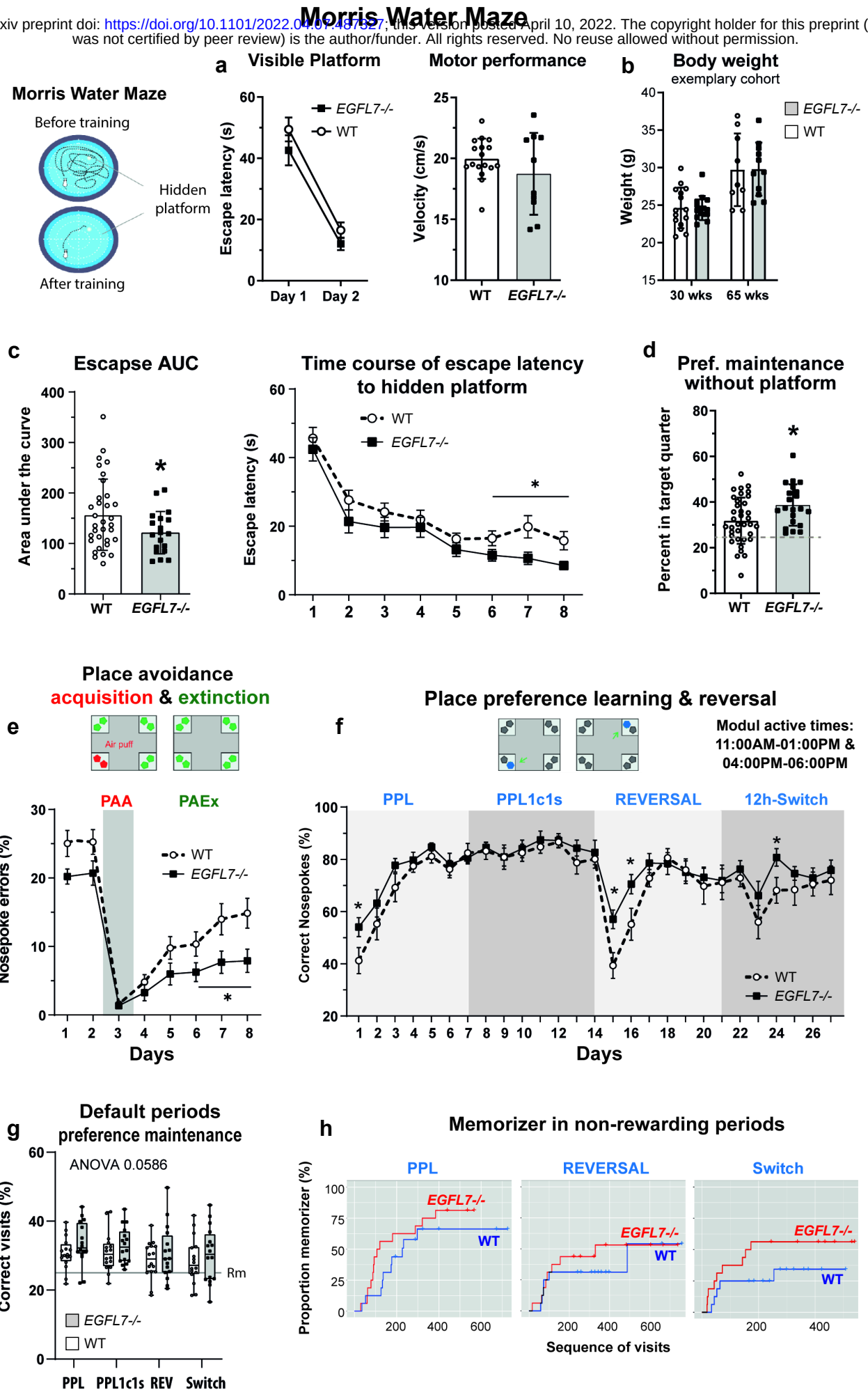

Figure 9

# IntelliCage in old *EGFL7 fl/fl;EIIa-Cre* versus *EGFL7 fl/fl*